



**Abstract**

The complexity of organic matter (OM) degradation mechanisms represents a significant challenge for developing biogeochemical models to quantify the role of aquatic sediments in the climate system. The common representation of OM by carbohydrates formulated as  $\text{CH}_2\text{O}$  in models comes with the assumption that its degradation by fermentation produces equimolar amounts of methane ( $\text{CH}_4$ ) and dissolved inorganic carbon (DIC). To test the validity of this assumption, we modeled using reaction-transport equations vertical profiles of the concentration and isotopic composition ( $\delta^{13}\text{C}$ ) of  $\text{CH}_4$  and DIC in the top 25 cm of the sediment column from two lake basins, one whose hypolimnion is perennially oxygenated and one with seasonal anoxia. Our results reveal that methanogenesis only occurs via hydrogenotrophy in both basins. Furthermore, we calculate, from  $\text{CH}_4$  and DIC production rates associated with methanogenesis, that the fermenting OM has an average carbon oxidation state (COS) below  $-0.9$ . Modeling solute porewater profiles reported in the literature for four other seasonally anoxic lake basins also yields negative COS values. Collectively, the mean ( $\pm\text{SD}$ ) COS value of  $-1.4 \pm 0.3$  for all the seasonally anoxic sites is much lower than the value of zero expected from carbohydrates fermentation. We conclude that carbohydrates do not adequately represent the fermenting OM and that the COS should be included in the formulation of OM fermentation in models applied to lake sediments. This study highlights the need to better characterize the labile OM undergoing mineralization to interpret present-day greenhouse gases cycling and predict its alteration under environmental changes.

38

**Plain Language Summary**

Organic matter in aquatic sediments is a complex mixture of mainly uncharacterized molecules and can be converted to greenhouse gases, for example methane and carbon dioxide, which can be released into the atmosphere. In current models, organic matter is represented by carbohydrates whose fermentation in oxygen-depleted sediments produces equal amount of methane and carbon dioxide. In this study, we estimated the production rates of methane and carbon dioxide during fermentation in lake sediments using concentration data and carbon isotopes of these greenhouse gases. Our results show that fermentation in the sediment of the deepest parts of the lake produces more methane than carbon dioxide, and that their relative

48 production rates vary across sites. Hence, carbohydrates are not well-suited to represent organic  
49 matter in current models. We therefore propose a new formulation for organic matter  
50 fermentation in aquatic sediments to better quantify greenhouse gases release. A more precise  
51 formulation for organic matter fermentation in aquatic sediments is crucial to better quantify  
52 current greenhouse gas emissions as well as their fate under global climate change.

## 53 **1 Introduction**

54 Significant proportions of atmospheric methane (CH<sub>4</sub>) and carbon dioxide (CO<sub>2</sub>), two  
55 powerful greenhouse gases, are thought to originate from freshwater lake sediments (Wuebbles  
56 and Hayhoe 2002; Bastviken et al., 2004; Turner et al., 2015), but large uncertainties remain  
57 concerning their contribution to the global CO<sub>2</sub> and CH<sub>4</sub> budgets (Saunio et al., 2016). The role  
58 of these waterbodies in the global carbon (C) budget has been acknowledged for more than a  
59 decade (Cole et al. 2007). Especially in the lake-rich boreal region, lakes are hotspots of CO<sub>2</sub> and  
60 CH<sub>4</sub> release (Hastie et al., 2018; Wallin et al., 2018) and intensive sites of terrestrial C  
61 processing (Holgerson and Raymond, 2016; Staehr et al., 2012). Using high-resolution satellite  
62 imagery, Verpoorter et al. (2014) estimated to about 27 million the number of lakes larger than  
63 0.01 km<sup>2</sup> on Earth and reported that the highest lake concentration and surface area are found in  
64 boreal regions. Boreal lakes, which are typically small and shallow, are known to store large  
65 amounts of organic C, to warm up quickly, and to develop anoxic hypolimnia in the warm season  
66 (Schindler et al., 1996; Sabrekov et al., 2017). Owing to the great abundance of boreal lakes,  
67 their sensitivity to climate change and foreseen important role in the global C cycle, there is a  
68 need to further develop process-based models to better quantify C processing reactions in these  
69 lakes and their alteration under warming (Saunio et al., 2016).

70 In aquatic environments, CH<sub>4</sub> is mainly produced (methanogenesis) in the sediment along  
71 with CO<sub>2</sub> at depths where most electron acceptors (EAs) are depleted (Conrad, 1999; Corbett et  
72 al., 2013). During its upward migration to the atmosphere, CH<sub>4</sub> is partly aerobically or  
73 anaerobically oxidized to CO<sub>2</sub> (methanotrophy) in the upper strata of the sediments and in the  
74 water column (Bastviken et al., 2008; Raghoebarsing et al. 2006; Beal et al. 2009; Ettwig et al.  
75 2010; Egger et al. 2015). The oxidation of organic matter (OM) by EAs such as O<sub>2</sub>, NO<sub>3</sub><sup>-</sup>,  
76 Fe(III), Mn(IV), SO<sub>4</sub><sup>2-</sup> and humic substances, as well as the partial fermentation of high  
77 molecular weight organic matter (HMW OM) into lower molecular weight organic matter (LMW

78 OM) are also potential sources of CO<sub>2</sub> in the sedimentary environment (Corbett et al., 2015).  
79 Predicting fluxes of CH<sub>4</sub> and CO<sub>2</sub> from the aquatic sediments and water column to the  
80 atmosphere is challenging considering the various transport processes and chemical and  
81 microbially-mediated reactions implicated and the complexity of natural OM which serves as  
82 substrate (Natchimuthu et al., 2017).

83 Process-based geochemical models taking into account both the numerous  
84 biogeochemical reactions involving C and transport processes are powerful tools able to interpret  
85 present-day sediment, porewater and water-column profiles of C species and offer a great  
86 potential to forecast changes in cycling of this element under variable environmental scenarios  
87 (Wang and Van Cappellen 1996; Arndt et al., 2013; Paraska et al., 2014; Sauniois et al., 2016).  
88 Nonetheless, the performance of these models depends on the correct formulation of the OM  
89 mineralization reactions, particularly in terms of the metabolizable organic compounds involved.  
90 Up to now, carbohydrates, represented as the simple chemical formula CH<sub>2</sub>O (or C<sub>6</sub>H<sub>12</sub>O<sub>6</sub>),  
91 whose average carbon oxidation state (COS) is zero, are commonly assumed to be representative  
92 of the bulk of metabolizable OM, including the substrates involved in fermentation reactions  
93 (e.g., Arndt et al., 2013; Paraska et al., 2014; Arning et al., 2016 and references therein). The  
94 capacity of CH<sub>2</sub>O to represent adequately the ensemble of labile organic compounds is,  
95 nevertheless, becoming increasingly questioned in the literature given the variety and complexity  
96 of organic molecules present in the environment (Alperin et al., 1994; Berelson et al., 2005;  
97 Jørgensen and Parkes, 2010; Burdige and Komada, 2011; Clayer et al., 2016). Based on the  
98 observation that methanogenesis produced CH<sub>4</sub> three times faster than CO<sub>2</sub> in the sediments of a  
99 boreal, sporadically anoxic lake basin, Clayer et al. (2018) concluded that the fermenting OM  
100 had a markedly negative COS value of -1.9. This COS value corresponds more closely to a  
101 mixture of fatty acids and fatty alcohols than to carbohydrates (e.g., CH<sub>2</sub>O), which would have  
102 yielded equivalent CH<sub>4</sub> and CO<sub>2</sub> production rates. The low COS value of metabolizable OM in  
103 the sediment layer where methanogenesis occurred in this lake has been attributed to the nearly  
104 complete consumption of the most labile organic components (e.g., carbohydrates, proteins)  
105 during its downward transport through the water column and the upper sediment layers, thus  
106 leaving only material of lower lability such as fatty acids and fatty alcohols available for  
107 methanogenesis. Such interpretation, however, must be validated by investigating other lakes  
108 before revising the formulation of the fermenting OM used in diagenetic models in order to

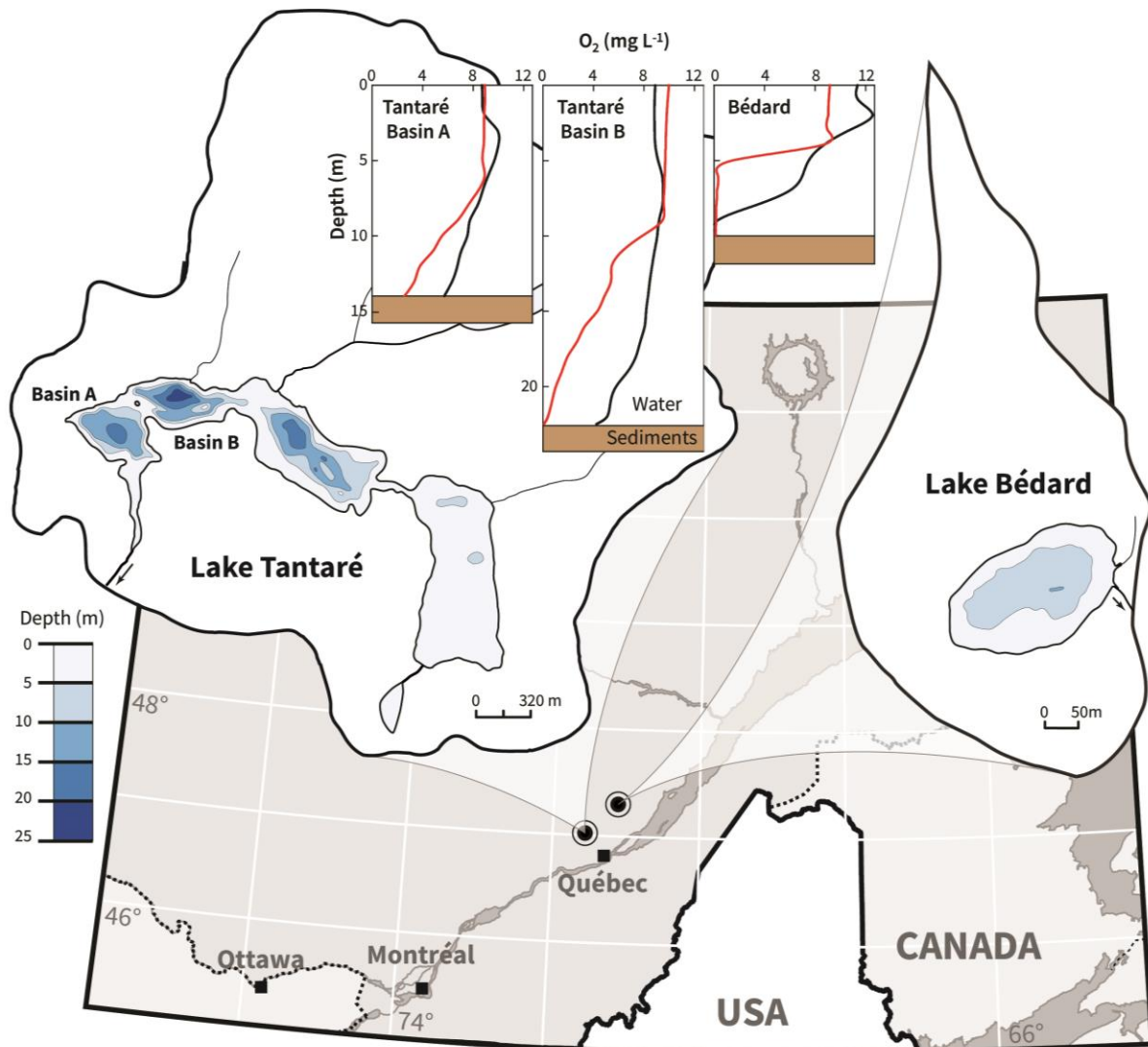
109 improve model predictions of C cycling, including greenhouse gases production and emission  
110 from these environments.

111 In this study, centimeter-scale vertical porewater profiles of the concentrations and of the  
112 stable carbon isotope ratios ( $\delta^{13}\text{C}$ ) of  $\text{CH}_4$  and dissolved inorganic carbon (DIC), as well as those  
113 of the concentrations of EAs were obtained in the hypolimnetic sediments of two additional  
114 boreal lake basins showing contrasted  $\text{O}_2$  dynamics: one whose hypolimnion remains perennially  
115 oxygenated and the other whose hypolimnion becomes anoxic for several months annually.  
116 Reaction-transport equations are used to quantify the rates of each OM mineralization pathway  
117 and estimate the COS of the substrates fermenting in the sediments. Additional insight into the  
118 COS of the fermenting OM in lakes is also provided by applying these equations to similar  
119 porewater solute concentration profiles gathered from the scientific literature or from our data  
120 repository.

## 121 **2 Materials and Methods**

### 122 2.1 Sites and sample collection

123 This study was carried out in two small, dimictic, oligotrophic and headwater lakes  
124 located within 50 km from Québec City, Eastern Canada and having fully forested and  
125 uninhabited watersheds (Fig. 1). Lake Tantaré ( $47^\circ 04' \text{N}$ ,  $71^\circ 32' \text{W}$ ) is part of the Tantaré  
126 Ecological Reserve and has four basins connected by shallow channels and a total surface area of  
127  $1.1 \text{ km}^2$ . Lake Bédard ( $47^\circ 16' \text{N}$ ,  $71^\circ 07' \text{W}$ ), lying in the protected Montmorency Forest,  
128 comprises only one small ( $0.05 \text{ km}^2$ ) basin. The samples for this study were collected at the  
129 deepest sites of Lake Bédard (10 m) and of the westernmost basin of Lake Tantaré (15 m),  
130 thereafter referred to as Basin A of Lake Tantaré to remain consistent with our previous studies  
131 (e.g., Couture et al., 2008; Clayer et al., 2016). These two sampling sites were selected based on  
132 their contrasting  $\text{O}_2$  regimes (Fig. 1): Lake Bédard develops an anoxic hypolimnion early in the  
133 summer (D'arcy, 1993), whereas the hypolimnion of Lake Tantaré Basin A is perennially  
134 oxygenated (Couture et al., 2008). The  $\text{O}_2$  diffusion depth in the sediments of Lake Tantaré  
135 Basin A, as measured with a microelectrode, does not exceed 4 mm (Couture et al., 2016).



136 **Figure 1:** Location map and bathymetry of Lakes Tantaré and Bédard. The bathymetric map of Lake Tantaré was  
 137 reproduced from the map C-9287 of the Service des eaux de surface of the Québec Ministry of Environment. The map of  
 138 Lake Bédard was reproduced from D'Arcy (1993). Dioxygen concentrations in the water column of Lake Tantaré basins  
 139 A and B, and of Lake Bédard are given for June (black lines) and October (red lines).

140 Sediment porewater samples were acquired by *in situ* dialysis in October 2015 with  
 141 peepers (Hesslein, 1976; Carignan et al., 1985) deployed by divers within a 25-m<sup>2</sup> area at the  
 142 deepest site of each lake basin. Bottom water O<sub>2</sub> concentrations were ~2.5 and < 0.1 mg L<sup>-1</sup> in  
 143 Lake Tantaré Basin A and in Lake Bédard, respectively. The acrylic peepers comprised two  
 144 columns of 4-mL cells, filled with ultrapure water, and covered by a 0.2- $\mu$ m Gelman HT-200  
 145 polysulfone membrane, which allowed porewater sampling from about 23–25 cm below the  
 146 sediment-water interface (SWI) to 5 cm above this interface (thereafter referred to as overlying  
 147 water) at a 1-cm depth resolution. Oxygen was removed from the peepers prior to their  
 148 deployment, as described by Laforte et al. (2005). Four peepers were left in the sediments of

149 each lake basin for at least 15 d, i.e., a longer time period than that required for solute  
 150 concentrations in the peeper cells to reach equilibrium with those in the porewater (5–10 d;  
 151 Hesslein, 1976; Carignan et al., 1985). At least three independent porewater profiles of pH, of  
 152 the concentrations of CH<sub>4</sub>, DIC, acetate, NO<sub>3</sub><sup>-</sup>, SO<sub>4</sub><sup>2-</sup>, Fe and Mn, and of the δ<sup>13</sup>C of CH<sub>4</sub> and DIC  
 153 were generated for the two sampling sites. In Lake Bédard, samples were also collected to  
 154 determine three porewater profiles of sulfide concentrations (ΣS(-II)). After peeper retrieval,  
 155 samples (0.9–1.9 mL) for CH<sub>4</sub> and DIC concentrations and δ<sup>13</sup>C measurements were collected  
 156 within 5 minutes from the peeper cells with He-purged polypropylene syringes. They were  
 157 injected through rubber septa into He-purged 3.85-mL exetainers (Labco Limited), after removal  
 158 of a volume equivalent to that of the collected porewater. The exetainers were preacidified with  
 159 40–80 μL of HCl 1N to reach a final pH ≤ 2. The protocols used to collect and preserve water  
 160 samples for the other solutes are given by Laforte et al. (2005).

## 161 2.2 Analyses

162 Concentrations and carbon isotopic composition of CH<sub>4</sub> and DIC were measured as  
 163 described by Clayer et al. (2018). Briefly, the concentrations were analyzed within 24 h of  
 164 peeper retrieval by gas chromatography with a precision better than 4 % and detection limits  
 165 (DL) of 2 μM and 10 μM for CH<sub>4</sub> and DIC, respectively. The <sup>13</sup>C/<sup>12</sup>C abundance ratios of CH<sub>4</sub>  
 166 and CO<sub>2</sub> were determined by Mass Spectrometry with a precision of ± 0.2 ‰ when 25 μmol of  
 167 an equimolar mixture of CH<sub>4</sub> and CO<sub>2</sub> was injected, and results are reported as:

$$\delta^{13}\text{C} = 1000 \left( \frac{\left( \frac{{}^{13}\text{C}_{\text{solute}}}{{}^{12}\text{C}_{\text{solute}}} \right)_{\text{sample}}}{\left( \frac{{}^{13}\text{C}}{{}^{12}\text{C}} \right)_{\text{standard}}} - 1 \right) \quad (1)$$

168 where the subscript solute stands for CH<sub>4</sub> or DIC and the reference standard is Vienna Pee Dee  
 169 Belemnite (VPDB). Acetate concentration was determined by ion chromatography (DL of 1.4  
 170 μM) and those of Fe, Mn, NO<sub>3</sub><sup>-</sup>, SO<sub>4</sub><sup>2-</sup> and ΣS(-II), as given by Laforte et al. (2005).

## 171 2.3 Modeling of porewater solutes and the reaction network

172 The computer program WHAM 6 (Tipping, 2002) was used, as described by Clayer et al.  
 173 (2016), to calculate the speciation of porewater cations and anions. The solute activities thus

174 obtained, together with solubility products ( $K_s$ ), were used to calculate saturation index values  
 175 ( $SI = \log IAP/K_s$ , where IAP is the ion activity product).

176 The following one-dimensional mass-conservation equation (Boudreau, 1997):

$$\frac{\partial}{\partial x} \left( \varphi D_s \frac{\partial [\text{solute}]}{\partial x} \right) + \varphi \alpha_{\text{Irrigation}} ([\text{solute}]_{\text{tube}} - [\text{solute}]) + R_{\text{net}}^{\text{solute}} = 0 \quad (2)$$

177 was used to model the porewater profiles of  $\text{CH}_4$ , DIC,  $\text{O}_2$ , Fe and  $\text{SO}_4^{2-}$ , assuming steady state  
 178 and negligible solute transport by bioturbation and advection (Clayer et al., 2016). In this  
 179 equation,  $[\text{solute}]$  and  $[\text{solute}]_{\text{tube}}$  denote a solute concentration in the porewater and in the  
 180 animal tubes (assumed to be identical to that in the overlying water), respectively,  $x$  is depth  
 181 (positive downward),  $\varphi$  is porosity,  $D_s$  is the solute effective diffusion coefficient in sediments,  
 182  $\alpha_{\text{Irrigation}}$  is the bioirrigation coefficient, and  $R_{\text{net}}^{\text{solute}}$  (in  $\text{mol cm}^{-3}$  of wet sediment  $\text{s}^{-1}$ ) is the  
 183 solute net production rate (or consumption rate if  $R_{\text{net}}^{\text{solute}}$  is negative).  $D_s$  was assumed to be  
 184  $\varphi^2 D_w$  (Ullman and Aller, 1982), where  $D_w$  is the solute tracer diffusion coefficient in water. The  
 185 values of  $D_w$ , corrected for in situ temperature (Clayer et al., 2018), were  $9.5 \times 10^{-6} \text{ cm}^2 \text{ s}^{-1}$ ,  $6.01$   
 186  $\times 10^{-6} \text{ cm}^2 \text{ s}^{-1}$  and  $1.12 \times 10^{-5} \text{ cm}^2 \text{ s}^{-1}$  for  $\text{CH}_4$ ,  $\text{HCO}_3^-$  and  $\text{CO}_2$ , respectively. The values of  
 187  $\alpha_{\text{Irrigation}}$  in Lake Tantaré Basin A were calculated as in Clayer et al. (2016), based on an  
 188 inventory of benthic animals (Hare et al., 1994), and were assumed to be 0 in Lake Bédard since  
 189 its bottom water was anoxic (Fig. 1).

190 The  $R_{\text{net}}^{\text{solute}}$  values were determined from the average ( $n = 3$  or  $4$ ) solute concentration  
 191 profiles by numerically solving Eq. (2) with the computer code PROFILE (Berg et al., 1998).  
 192 The boundary conditions were the solute concentrations at the top and at the base of the  
 193 porewater profiles. In situ porewater  $\text{O}_2$  profiles were not measured in Lake Tantaré Basin A. For  
 194 modeling this solute with PROFILE, we assumed that the  $[\text{O}_2]$  in the overlying water was  
 195 identical to that measured in the lake bottom water and equal to 0 below 0.5 cm (based on  $\text{O}_2$   
 196 penetration depth; Couture et al., 2016). This procedure provides a rough estimate of  $R_{\text{net}}^{\text{O}_2}$  at the  
 197 same vertical resolution as for the other solutes. The code PROFILE yields a discontinuous  
 198 profile of discrete  $R_{\text{net}}^{\text{solute}}$  values over depth intervals (zones) which are objectively selected by  
 199 using the least square criterion and statistical F-testing (Berg et al., 1998). The fluxes of solute  
 200 transport across the SWI due to diffusion and bioirrigation are also estimated by PROFILE. In

201 order to estimate the variability in  $R_{\text{net}}^{\text{solute}}$  related to heterogeneity within the 25-m<sup>2</sup> sampling  
 202 area, additional  $R_{\text{net}}^{\text{solute}}$  values were obtained by modeling the average profiles whose values  
 203 were increased or decreased by one standard deviation. This variability generally ranges between  
 204 2 and 10 fmol cm<sup>-3</sup> s<sup>-1</sup>.

205 The main reactions retained in this study to describe carbon cycling in the sediments of  
 206 the two lake basins are shown in Table 1. Once oxidants are depleted, fermentation of  
 207 metabolizable OM (r1) can yield acetate, CO<sub>2</sub> and H<sub>2</sub>. The partial degradation of high molecular  
 208 weight OM (HMW OM) into lower molecular weight OM (LMW OM) can also produce CO<sub>2</sub>  
 209 (r2, Corbett et al., 2013; Corbett et al., 2015). Acetoclasty (r3) and hydrogenotrophy (r4) yield  
 210 CH<sub>4</sub>. Moreover, CH<sub>4</sub> (r5) and OM (r6) can be oxidized to CO<sub>2</sub> when electron acceptors such as  
 211 O<sub>2</sub>, Fe(III) and SO<sub>4</sub><sup>2-</sup> are present. Note that the electron acceptors (EAs) NO<sub>3</sub><sup>-</sup> and Mn  
 212 oxyhydroxides can be neglected in these two lake basins (Feyte et al., 2012; Clayer et al., 2016)  
 213 as well as the precipitation of metal carbonates whose saturation index values are negative  
 214 (SI ≤ -1.5) except for siderite (r7) in Lake Bédard (SI = 0.0 to 0.7). Lastly, sulfide oxidation by  
 215 iron oxides (r8), which can be a source of SO<sub>4</sub><sup>2-</sup> and H<sub>2</sub> (Holmkvist et al., 2011; Clayer et al.,  
 216 2018), is also considered.

217 From Table 1, the net rate of CH<sub>4</sub> production,  $R_{\text{net}}^{\text{CH}_4}$ , in the sediments is:

$$R_{\text{net}}^{\text{CH}_4} = R_3 + R_4 - R_5 \quad (3)$$

218 where  $R_3$  and  $R_4$  are the rates of acetoclastic (r3) and hydrogenotrophic (r4) production of CH<sub>4</sub>,  
 219 respectively, and  $R_5$  is the rate of DIC production due to CH<sub>4</sub> oxidation (r5). The net rate of DIC  
 220 production,  $R_{\text{net}}^{\text{DIC}}$ , can be expressed as:

$$R_{\text{net}}^{\text{DIC}} = R_1 + R_2 + R_3 - R_4 + R_5 + R_6 - R_7 \quad (4)$$

221 where  $R_1$ ,  $R_2$  and  $R_6$  are the rates of DIC production due to complete fermentation of labile OM  
 222 (r1), partial fermentation of HMW OM (r2) and OM oxidation (r6), respectively, and  $R_7$  is the  
 223 rate of DIC removal by siderite precipitation (r7). It can also be written that:

$$R_{\text{net}}^{\text{Ox}} = -2R_5 - R_6 \quad (5)$$

224 where  $R_{\text{net}}^{\text{Ox}}$  is the net reaction rate of all the oxidants (O<sub>2</sub>, Fe(III) and SO<sub>4</sub><sup>2-</sup>) consumption. For  
 225 simplicity,  $R_{\text{net}}^{\text{Ox}}$  is expressed in equivalent moles of O<sub>2</sub> consumption rate, taking into account

226 that  $\text{SO}_4^{2-}$  and Fe(III) have twice and one quarter the oxidizing capacity of  $\text{O}_2$ , respectively. In  
 227 practice, the value of  $R_{\text{net}}^{\text{Ox}}$  was calculated by adding those of  $R_{\text{net}}^{\text{O}_2}$ ,  $\frac{1}{4}R_{\text{net}}^{\text{Fe(III)}}$  and  $2R_{\text{net}}^{\text{SO}_4^{2-}}$  where  
 228  $R_{\text{net}}^{\text{O}_2}$ ,  $R_{\text{net}}^{\text{Fe(III)}}$  and  $R_{\text{net}}^{\text{SO}_4^{2-}}$  were estimated with PROFILE. In this calculation, we assumed that all  
 229 dissolved Fe is in the form of Fe(II), and that the rate of Fe(II) consumption through reactions r7  
 230 is negligible compared to those associated with reactions r5 and r6. Under these conditions,  
 231  $R_{\text{net}}^{\text{Fe(III)}} = -R_{\text{net}}^{\text{Fe}}$ .

232 **Table 1: Reactions (r1–r8) considered, their reaction rates ( $R_1$ – $R_8$ ) and carbon isotopic fractionation factors ( $\alpha_1$ – $\alpha_7$ ).**

Description	Reaction	ID
<b>CO<sub>2</sub> production due to complete fermentation of labile OM<sup>a</sup></b>		
	$\text{C}_x\text{H}_y\text{O}_z + (x + v_1 - z)\text{H}_2\text{O} \xrightarrow[\alpha_1]{R_1} \left(\frac{x - v_1}{2}\right)\text{CH}_3\text{COOH} + v_1\text{CO}_2 + \left(\frac{y}{2} - z + 2v_1\right)\text{H}_2$	r1
<b>CO<sub>2</sub> production due to partial fermentation of HMW OM<sup>a,b</sup></b>		
	$v_2\text{HMW OM} \xrightarrow[\alpha_2]{R_2} v_3\text{LMW OM} + v_4\text{CO}_2$	r2
<b>Methanogenesis via</b>		
acetoclasty	$\text{CH}_3\text{COOH} \xrightarrow[\alpha_3]{R_3} \text{CH}_4 + \text{CO}_2$	r3
hydrogenotrophy	$\text{CO}_2 + 4\text{H}_2 \xrightarrow[\alpha_4]{R_4} \text{CH}_4 + 2\text{H}_2\text{O}$	r4
<b>CO<sub>2</sub> production due to</b>		
methanotrophy	$\text{CH}_4 + 2\text{Oxidants} \xrightarrow[\alpha_5]{R_5} \text{CO}_2 + 2\text{Reducers}$	r5
OM oxidation	$\text{OM} + \text{Oxidant} \xrightarrow[\alpha_6]{R_6} \text{CO}_2 + \text{Reducer}$	r6
<b>Precipitation of siderite</b>	$\text{Fe}^{2+} + \text{CO}_2 + \text{H}_2\text{O} \xrightarrow[\alpha_7]{R_7} \text{FeCO}_{3(s)} + 2\text{H}^+$	r7
<b>H<sub>2</sub> production through a Fe-S cryptic cycle<sup>a,c</sup></b>		
	$(16 + v_5)\text{H}_2\text{S} + 8\text{FeOOH} \xrightarrow{R_8} 8\text{FeS}_2 + v_5\text{SO}_4^{2-} + (4 + 4v_5)\text{H}_2 + (16 - 4v_5)\text{H}_2\text{O} + 2v_5\text{H}^+$	r8

233 <sup>a</sup> where  $v_1$  can have any value between 0 and x, values for  $v_2$ – $v_4$  are unknown and  $v_5$  can have any value between 0  
 234 and 1.

235 <sup>b</sup> HMW OM and LMW OM designate high and lower molecular weight organic matter, respectively.

236 <sup>c</sup> adapted from Holmkvist et al. (2011)

237 2.4 Modeling of the  $\delta^{13}\text{C}$  profiles

238 The  $\delta^{13}\text{C}$  profiles of  $\text{CH}_4$  ( $\delta^{13}\text{C}\text{-CH}_4$ ) and DIC ( $\delta^{13}\text{C}\text{-DIC}$ ) were simulated with a  
 239 modified version of Eq. 1 (Clayer et al., 2018):

$$\delta^{13}\text{C} = 1000 \left( \frac{\left( \frac{[^{13}\text{C}]}{[\text{C}]} \right)_{\text{sample}}}{\left( \frac{[^{13}\text{C}]}{[^{12}\text{C}]} \right)_{\text{standard}}} - 1 \right) \quad (6)$$

240 where  $[\text{C}]$  is the total  $\text{CH}_4$  or DIC concentration ( $[^{12}\text{C}]$  can be replaced by  $[\text{C}]$  since  $\sim 99\%$  of C is  
 241  $^{12}\text{C}$ ), and  $[^{13}\text{C}]$  is the isotopically heavy  $\text{CH}_4$  or DIC concentration. Equation 6 allows  
 242 calculating a  $\delta^{13}\text{C}$  profile once the depth distributions of  $[^{13}\text{C}]$  and  $[\text{C}]$  are known. This  
 243 information is obtained by solving the mass-conservation equations of C and  $^{13}\text{C}$  for  $\text{CH}_4$  and  
 244 DIC. The one-dimensional mass-conservation of  $[\text{C}]$  is given by Eq. 2 where [solute] is replaced  
 245 by  $[\text{C}]$ , whereas that for  $[^{13}\text{C}]$  is the following modified version of Eq. 2 (Clayer et al., 2018):

$$\frac{\partial}{\partial x} \left( \varphi \frac{D_s}{f} \frac{\partial [^{13}\text{C}]}{\partial x} \right) + \varphi \alpha_{\text{irrigation}} ([^{13}\text{C}]_{\text{tube}} - [^{13}\text{C}]) + \sum_{i=1}^5 \frac{R_i}{\alpha_i} \left( \frac{\delta^{13}\text{C}_i^{\text{reactant}}}{1000} + 1 \right) \left( \frac{[^{13}\text{C}]}{[^{12}\text{C}]} \right)_{\text{standard}} = 0 \quad (7)$$

246 where  $f$ , the molecular diffusivity ratio, is the diffusion coefficient of the regular solute divided  
 247 by that of the isotopically heavy solute,  $\alpha_i$  is the isotope fractionation factor in reaction  $r_i$ , and  
 248  $\delta^{13}\text{C}_i^{\text{reactant}}$  is the  $\delta^{13}\text{C}$  of the reactant leading to the formation of the solute ( $\text{CH}_4$  or DIC) in  
 249 reaction  $r_i$ . Input and boundary conditions used to numerically solve Eqs 2 and 7 for  $[\text{C}]$  and  
 250  $[^{13}\text{C}]$ , respectively, via the `bvp5c` function of MATLAB<sup>®</sup> are described in section 3.4 and in  
 251 section S2 of the Supporting Information (SI).

252 The goodness of fit of the model was assessed with the norm of residuals ( $N_{\text{res}}$ ):

$$N_{\text{res}} = \sqrt{\sum_{x=0.5}^{22.5} (\delta^{13}\text{C}_m - \delta^{13}\text{C}_s)^2} \quad (8)$$

253 where  $\delta^{13}\text{C}_m$  and  $\delta^{13}\text{C}_s$  are the measured and simulated  $\delta^{13}\text{C}$  values, respectively. The norm of  
 254 residuals ( $N_{\text{res}}$ ) varies between 0 and infinity with smaller numbers indicating better fits.

## 255 2.5 Data treatment of other data sets

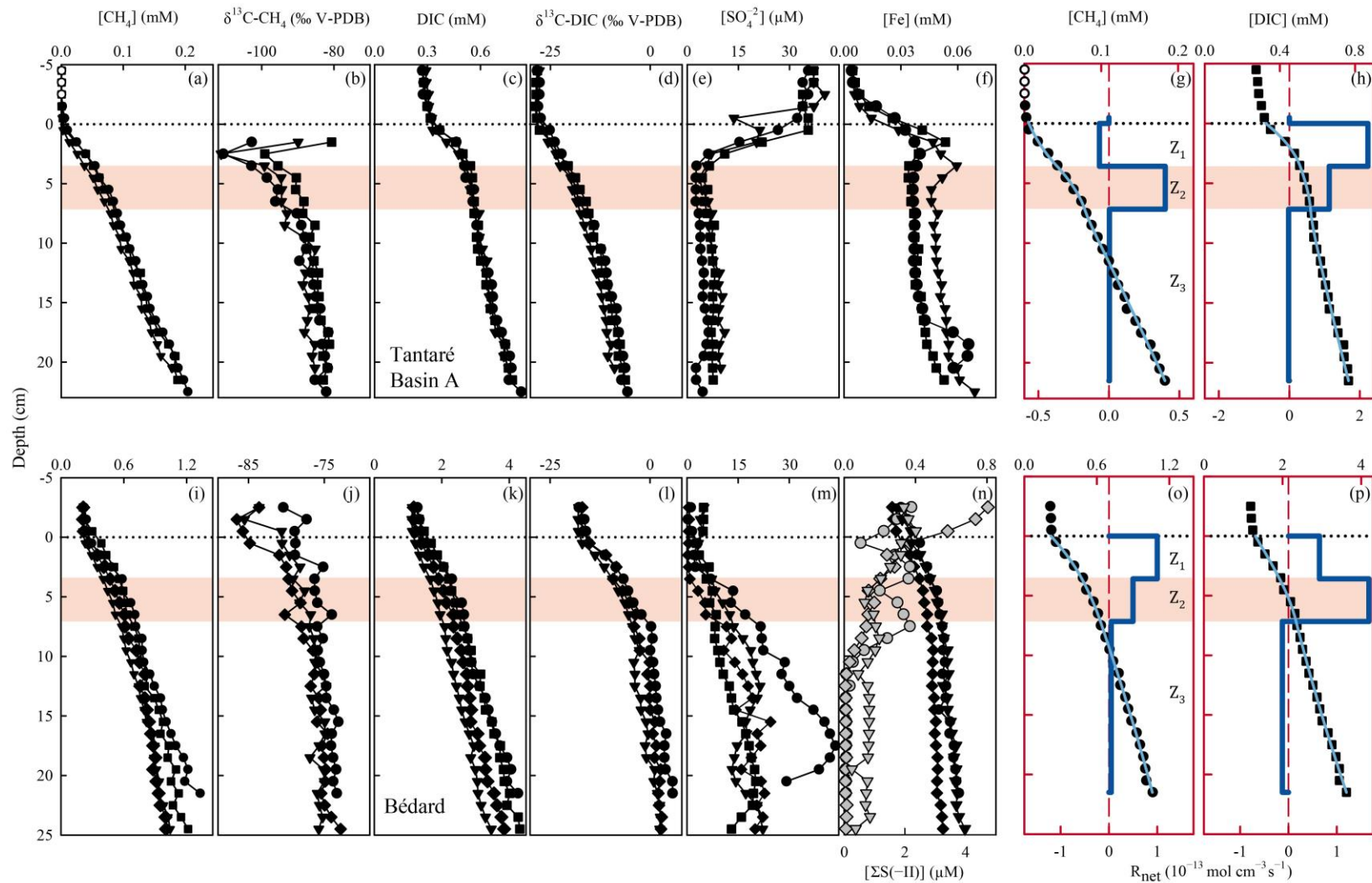
256 To better assess the COS of the fermenting OM in lakes, relevant sets of porewater  
257 concentration profiles ( $\text{CH}_4$ , DIC, EAs, Ca) available from the literature or from our data  
258 repository have been modeled with the code PROFILE, as described in section 2.3, to extract  
259 their  $R_{\text{net}}^{\text{CH}_4}$ ,  $R_{\text{net}}^{\text{DIC}}$  and  $R_{\text{net}}^{\text{Ox}}$  profiles. These porewater datasets, described in section S3 of the SI,  
260 had been generated by sampling porewater in the hypolimnetic sediments of: i) Lake Bédard and  
261 Basin A of Lake Tantaré, at other dates than for this study (Clayer et al, 2016); ii) Basin B of  
262 Lake Tantaré (adjacent to Basin A; Fig 1), on four occasions (Clayer et al., 2016; 2018); iii)  
263 Williams Bay of Jacks Lake ( $44^\circ 41' \text{ N}$ ,  $78^\circ 02' \text{ W}$ ), located in Ontario, Canada, on the edge of  
264 the Canadian Shield (Carignan and Lean 1991); iv) the southern basin of the alpine Lake Lugano  
265 ( $46^\circ 00' \text{ N}$ ,  $3^\circ 30' \text{ E}$ ) located in Switzerland, on two occasions (Lazzaretti-Ulmer and Hanselmann  
266 1999). All lake basins, except Basin A of Lake Tantaré develop an anoxic hypolimnion.

## 267 3 Results

### 268 3.1 Solute concentration profiles

269 Differences among the replicate profiles of  $\text{CH}_4$ , DIC,  $\text{SO}_4^{2-}$ ,  $\Sigma\text{S}(-\text{II})$  and Fe (Fig. 2) at  
270 the two sampling sites are generally small (except perhaps those of  $\text{SO}_4^{2-}$  in Lake Bédard) and  
271 should be mainly ascribed to spatial variability within the 25- $\text{m}^2$  sampling area. Indeed, the main  
272 vertical variations in the profiles are defined by several data points without the sharp  
273 discontinuities expected from sampling and handling artifacts. Note that the acetate  
274 concentrations, which were consistently low ( $< 2 \mu\text{M}$ ), are not shown.

275 The low Fe ( $< 5 \mu\text{M}$ ; Fig. 2f) and  $\text{CH}_4$  ( $< 2 \mu\text{M}$ ; Fig. 2a) concentrations as well as the  
276 relatively high  $\text{SO}_4^{2-}$  concentrations ( $36 \pm 2.1 \mu\text{M}$ ; Fig. 2e) in the sediment overlying water of  
277 Lake Tantaré Basin A are all consistent with the  $[\text{O}_2]$  ( $\sim 2.5 \text{ mg L}^{-1}$ ) measured in the bottom  
278 water and are indicative of oxic conditions at the sediment surface. The sharp Fe gradients near  
279 the SWI indicate an intense recycling of Fe oxyhydroxides (Fig. 2f; Clayer et al., 2016) and the  
280 concave-down curvatures in the  $\text{SO}_4^{2-}$  profiles (Fig. 2e) reveal  $\text{SO}_4^{2-}$  reduction near the SWI.



281 **Figure 2 :** Replicate porewater profiles of CH<sub>4</sub> (a and i), δ<sup>13</sup>C-CH<sub>4</sub> (b and j), DIC (c and k), δ<sup>13</sup>C-DIC (d and l), SO<sub>4</sub><sup>2-</sup> (e and m), Fe and ΣS(-II) (f and n), and  
 282 comparison of the modeled (blue lines) and average (n = 3) measured (symbols) concentration profiles of CH<sub>4</sub> (g and o) and DIC (h and p) in Lakes Tantaré Basin A (a-  
 283 284 285 h) and Bédard (i-p). Different symbols indicate data from different peepers and empty symbols are for concentrations below detection limit. The horizontal dotted line  
 indicates the sediment-water interface. The thick and thin blue lines represent the net solute reaction rate ( $R_{\text{net}}^{\text{solute}}$ ) and the modeled concentration profiles, respectively.  
 The red area fills correspond to the sediment zones Z2.

286 In contrast to Lake Tantaré Basin A, high Fe ( $> 200 \mu\text{M}$ ), measurable  $\text{CH}_4$  ( $> 200 \mu\text{M}$ )  
287 low  $\text{SO}_4^{2-}$  ( $2.7 \pm 1.4 \mu\text{M}$ ) and detectable  $\Sigma\text{S}(-\text{II})$  concentrations in the overlying waters of Lake  
288 Bédard (Fig. 2i, m and n) are consistent with anoxic conditions at the sediment surface. The  
289 absence of a sharp Fe gradient at the SWI in Lake Bédard suggests that Fe oxyhydroxides were  
290 not recycled in these sediments when porewater sampling occurred.

291 In the two lake basins,  $\text{SO}_4^{2-}$  concentrations reach a minimum between the SWI and 5 cm  
292 depth (Fig. 2e and m), and increase below these depths. Alongside, all Fe profiles show a slight  
293 increase downward (Fig. 2f and n) indicating that solid Fe(III) is reduced to produce dissolved  
294 Fe. In Lake Bédard, the  $\Sigma\text{S}(-\text{II})$  concentrations decrease from the SWI to  $\sim 10$  cm depth and  
295 remain relatively constant below that depth at  $0.08 \pm 0.06 \mu\text{M}$  for two of the profiles and at  
296  $0.71 \pm 0.18 \mu\text{M}$  for the other one (grey filled triangles in Fig. 2n).

297 The concentrations of  $\text{CH}_4$  ( $< 1.5 \text{ mM}$ ; Fig. 2a and i) are well below saturation at  $4^\circ\text{C}$  and  
298 *in situ* pressure (4.4–5.5 mM; Duan and Mao, 2006), implying that  $\text{CH}_4$  ebullition is a negligible  
299  $\text{CH}_4$  transport process. The  $\text{CH}_4$  values increases from  $< 2 \mu\text{M}$  in the overlying water to 0.18–  
300 0.20 mM at the base of the Lake Tantaré Basin A profiles (Fig. 2a), and from 0.2–0.5 mM to  
301 1.0–1.4 mM in those of Lake Bédard (Fig. 2i). The three  $\text{CH}_4$  profiles from Lake Tantaré Basin  
302 A (Fig. 2a) show a modest concave-up curvature in their upper part, close to the SWI, indicative  
303 of a net  $\text{CH}_4$  consumption, and a convex-up curvature in their lower part, typical of a net  $\text{CH}_4$   
304 production. Such trends, however, are not observed in Lake Bédard sediments. The  $\text{CH}_4$  profiles  
305 from this lake exhibit a convex-up curvature over the whole sediment column, although more  
306 pronounced in its upper part (Fig. 2i).

307 The DIC concentrations consistently increase from 0.27–0.32 mM and 1.2–1.5 mM in the  
308 sediment overlying water to 0.76–0.83 mM and 3.5–4.3 mM at the bottom of the profiles in Lake  
309 Tantaré Basin A and Lake Bédard, respectively (Fig. 2c and k). All DIC profiles show a similar  
310 shape with a slight concave-up curvature in their lower segment and a convex-up curvature in  
311 their upper portions.

### 312 3.2 Modeled $\text{CH}_4$ and DIC concentration profiles

313 The modeled  $[\text{CH}_4]$  and DIC profiles accurately fit the average ( $n = 3$  or  $4$ ) data points  
314 ( $r^2 > 0.996$  and  $r^2 > 0.998$  for  $\text{CH}_4$  and DIC, respectively; Fig. 2g,h,o and p). The  $R_{\text{net}}^{\text{CH}_4}$  profiles

315 reveal three zones in each lake basin numbered  $Z_1$ ,  $Z_2$  and  $Z_3$  from the sediment surface whose  
 316 boundaries match those defined by the  $R_{\text{net}}^{\text{DIC}}$  profiles. For Lake Tantaré Basin A,  $Z_1$  corresponds  
 317 to a net  $\text{CH}_4$  consumption and  $Z_2$  and  $Z_3$  to net  $\text{CH}_4$  production, with the highest rate in  $Z_2$  (Fig.  
 318 2g). In contrast, the three zones in Lake Bédard show net  $\text{CH}_4$  production with the highest rate in  
 319  $Z_1$  and the lowest in  $Z_3$  (Fig. 2o). The  $R_{\text{net}}^{\text{DIC}}$  profiles in both lake basins show a zone of net DIC  
 320 consumption below two zones of net DIC production with the highest rate values in the  $Z_1$  and  
 321  $Z_2$  for Lake Tantaré Basin A and Lake Bédard, respectively.

322 The  $R_{\text{net}}^{\text{CH}_4}$  and  $R_{\text{net}}^{\text{DIC}}$  profiles displayed in Figure 2 are, among all the possible solutions,  
 323 the ones that give the simplest rate profile while providing a satisfying explanation of the  
 324 averaged solute concentration profile as determined by statistical F-testing implemented in the  
 325 code PROFILE (P value  $\leq 0.001$  except for the  $R_{\text{net}}^{\text{DIC}}$  profile in Lake Bédard whose P value is  $\leq$   
 326 0.005). As an additional check of the robustness of the depth distribution of  $R_{\text{net}}^{\text{CH}_4}$  and  $R_{\text{net}}^{\text{DIC}}$   
 327 provided by PROFILE, we used another inverse model, i.e., Rate Estimation from  
 328 Concentrations (REC; Lettmann et al., 2012) to model the average  $\text{CH}_4$  and DIC profiles. Note  
 329 that the statistical method, implemented in REC to objectively select the depth distribution of the  
 330 net reaction rates, i.e., the Tikhonov regularization technique, differs from that of PROFILE.  
 331 Figure S1 (SI) shows that the two codes predicted mutually consistent  $R_{\text{net}}^{\text{CH}_4}$  and  $R_{\text{net}}^{\text{DIC}}$  profiles,  
 332 with rate values of similar magnitude. PROFILE was also used in this study to estimate  $R_{\text{net}}^{\text{SO}_4^{2-}}$ ,  
 333  $R_{\text{net}}^{\text{Fe}}$  and  $R_{\text{net}}^{\text{O}_2}$  in order to calculate the value of  $R_{\text{net}}^{\text{Ox}}$  in each zone at both sampling sites (see  
 334 section 2.3 for details). The modeled  $[\text{SO}_4^{2-}]$  and  $[\text{Fe}]$  profiles are not shown but, again, they  
 335 accurately fit the data points ( $r^2 > 0.983$ ). As expected from the contrasting  $\text{O}_2$  regimes of the  
 336 two lake basins,  $R_{\text{net}}^{\text{Ox}}$  values for Lake Tantaré Basin A were one to two orders of magnitude  
 337 higher than those for Lake Bédard. Note that  $R_{\text{net}}^{\text{O}_2}$  was by far the highest contributor to the value  
 338 of  $R_{\text{net}}^{\text{Ox}}$  in Lake Tantaré Basin A with values of  $-290$  and  $-72 \text{ fmol cm}^{-3} \text{ s}^{-1}$  in the  $Z_1$  and  $Z_2$ ,  
 339 respectively. The values of  $R_{\text{net}}^{\text{CH}_4}$ ,  $R_{\text{net}}^{\text{DIC}}$  and  $R_{\text{net}}^{\text{Ox}}$  estimated in each zone of each lake basins are  
 340 reported in Table 2.

341 **Table 2: Net production rates ( $R_{\text{net}}^{\text{solute}}$ ) of  $\text{CH}_4$ , DIC and oxidants obtained with the code PROFILE in the three  $\text{CH}_4$**   
 342 **consumption/production zones ( $Z_1$ ,  $Z_2$  and  $Z_3$ ) for both sampling sites.**

Sampling site ([O <sub>2</sub> ] in mg L <sup>-1</sup> )	Zones	Depth (cm)	$R_{\text{net}}^{\text{DIC}}$	$R_{\text{net}}^{\text{CH}_4}$	$R_{\text{net}}^{\text{Ox}}$
			(fmol cm <sup>-3</sup> s <sup>-1</sup> )		
Tantaré Basin A (2.5)	Z <sub>1</sub>	0–3.6	223	-7	-335
	Z <sub>2</sub>	3.6–7.2	113	39	-103
	Z <sub>3</sub>	7.2–21.5	-2	1	
Bédard (<0.1)	Z <sub>1</sub>	0–3.6	65	100	-6.5
	Z <sub>2</sub>	3.6–7.2	167	50	-4.5
	Z <sub>3</sub>	7.2–21.5	-13	5	

### 343 3.3 The $\delta^{13}\text{C}$ profiles

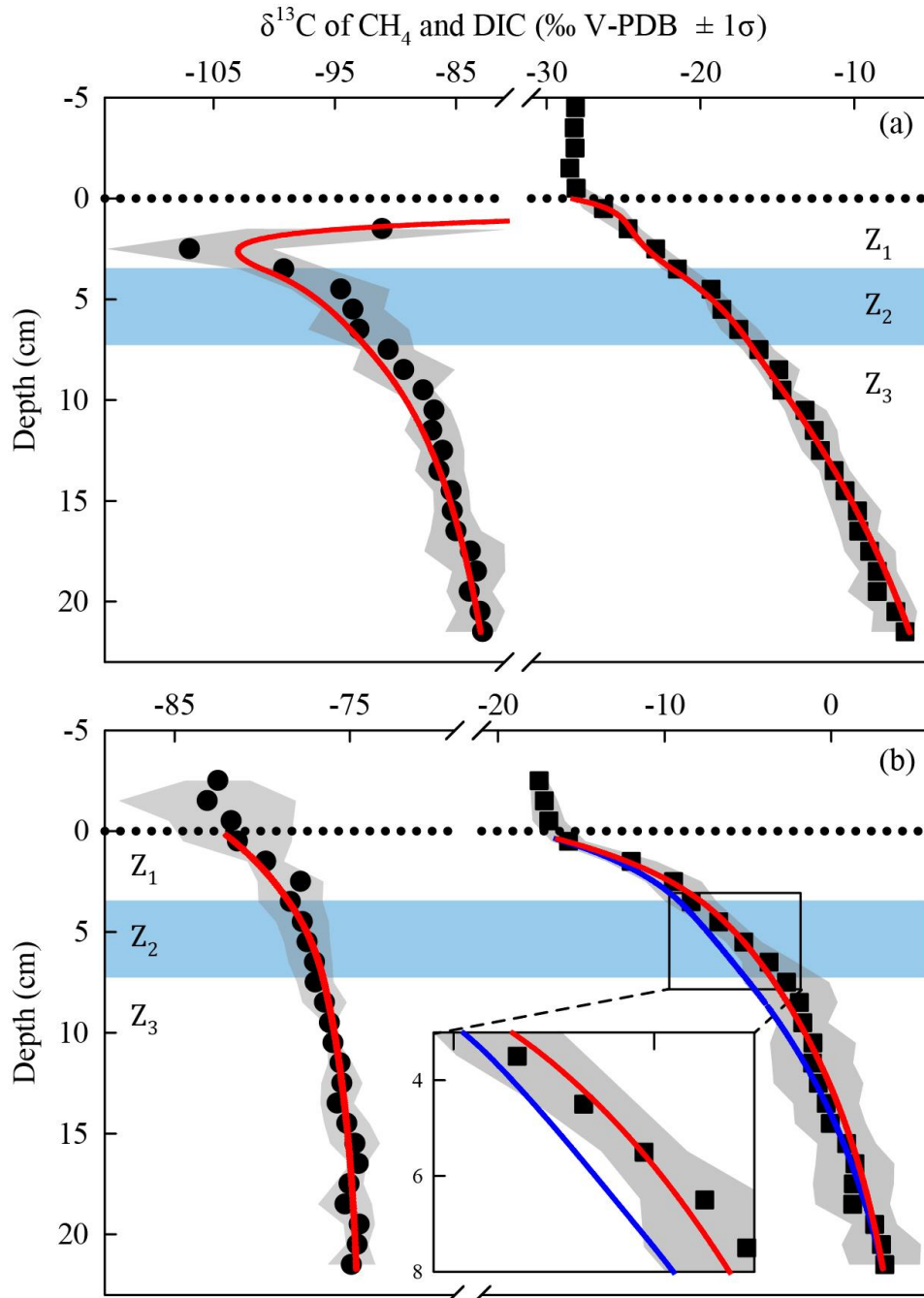
344 The  $\delta^{13}\text{C}$ -DIC values increase from  $-28.2 \pm 0.4$  ‰ and  $-17.2 \pm 0.7$  ‰ in the overlying  
 345 water to  $-5.1 \pm 1.0$  ‰ and  $3.6 \pm 1.7$  ‰ at the base of the profiles in Lake Tantaré Basin A and  
 346 Lake Bédard, respectively (Fig. 2d and l). Similarly, the  $\delta^{13}\text{C}$ - $\text{CH}_4$  values in Lake Bédard  
 347 increase steadily from  $-82.5 \pm 3.3$  ‰ in the overlying water to  $-74.0 \pm 1.5$  ‰ at 24.5 cm depth  
 348 (Fig. 2j). Regarding Lake Tantaré Basin A, the  $\text{CH}_4$  concentrations above 1.5 cm depth were too  
 349 low for their  $^{13}\text{C}/^{12}\text{C}$  ratio to be determined. Starting at 1.5 cm depth, the  $\delta^{13}\text{C}$ - $\text{CH}_4$  values first  
 350 decrease from  $-91.1 \pm 11.1$  ‰ to  $-107.0 \pm 6.8$  ‰ at 2.5 cm depth and then increase  
 351 progressively to  $-83.5 \pm 1.6$  ‰ at the base of the profiles (Fig. 2b). Note that a shift toward more  
 352 positive  $\delta^{13}\text{C}$ - $\text{CH}_4$  values upward, generally attributed to the oxidation of  $\text{CH}_4$  (Chanton et al.,  
 353 1997; Norđi et al., 2013), is only observed in the profiles of Lake Tantaré Basin A (Fig. 2b).

354 As shown in Fig. S2 (SI), the isotopic signatures of nearly all samples from the two lake  
 355 basins fall within the ranges reported for hydrogenotrophic methanogenesis, i.e.,  $\text{CO}_2$  reduction,  
 356 in a  $\delta^{13}\text{C}$ - $\text{CO}_2$  vs  $\delta^{13}\text{C}$ - $\text{CH}_4$  graph similar to that proposed by Whiticar (1999). Indeed, the values  
 357 of  $\delta^{13}\text{C}$ - $\text{CH}_4$  which are lower than -70 ‰ over the whole profiles in the two lake basins, and the  
 358 large difference (67 to 92 ‰) between the  $\delta^{13}\text{C}$  of gaseous  $\text{CO}_2$  ( $\delta^{13}\text{C}$ - $\text{CO}_2$ ) and  $\delta^{13}\text{C}$ - $\text{CH}_4$ ,  
 359 strongly contrast with the typical  $\delta^{13}\text{C}$ - $\text{CH}_4$  values ( $-68$  to  $-50$  ‰) and with the difference  
 360 between  $\delta^{13}\text{C}$ - $\text{CO}_2$  and  $\delta^{13}\text{C}$ - $\text{CH}_4$  (39 to 58 ‰) reported for acetoclasty (Whiticar, 1999). The  
 361  $\delta^{13}\text{C}$  results reported previously for another basin of Lake Tantaré (Basin B; Clayer et al., 2018)  
 362 show also in the hydrogenotrophy domain in Fig. S2.

363 3.4 Modeled  $\delta^{13}\text{C}$  profiles

364 In order to model the  $\delta^{13}\text{C}$  profiles with Eq. 6, accurate profiles of  $[\text{C}]$  and  $[\text{}^{13}\text{C}]$  need first  
365 to be determined by numerically solving Eqs. 2 and 7, respectively. The modeled profiles of  
366  $[\text{CH}_4]$  and DIC obtained with Eq. 2 replicated well the measured profiles of these two solutes  
367 when the depth distributions of  $R_{\text{net}}^{\text{CH}_4}$  or  $R_{\text{net}}^{\text{DIC}}$  provided by PROFILE (Table 2) and those of  $D_s$ ,  
368  $\alpha_{\text{Irrigation}}$  and  $\varphi$  were used as inputs in Eq. 2, and when measured  $\text{CH}_4$  or DIC concentrations at  
369 the top and bottom of the profiles were imposed as boundary conditions. Getting a truthful  
370 profile of  $[\text{}^{13}\text{C}]$  with Eq. 7 requires, however, accurate values of  $\delta^{13}\text{C}_i^{\text{reactant}}$ ,  $\alpha_i$ , and  $R_i$  for each  
371 of the reactions given in Table 1, and of  $f$  for both  $\text{CH}_4$  ( $f\text{-CH}_4$ ) and DIC ( $f\text{-DIC}$ ). The multi-step  
372 procedure followed to obtain the best  $[\text{}^{13}\text{C}]$  profiles for  $\text{CH}_4$  and DIC is described in section S2  
373 (SI). This modeling exercise revealed that  $R_3 = 0$  for all the zones in the sediments of both lake  
374 basins, thus confirming that practically all  $\text{CH}_4$  is produced through hydrogenotrophy, as inferred  
375 above from the  $\delta^{13}\text{C}$  values.

376 The best fits between the simulated and measured  $\delta^{13}\text{C}$  profiles of  $\text{CH}_4$  and DIC for Lake  
377 Tantaré Basin A and Lake Bédard (red lines in Fig. 3) were obtained with the  $f$ ,  $\alpha_i$  and  $R_i$  values  
378 displayed in Table 3. The optimal  $\alpha_i$  and  $f$  values were within the ranges reported in the literature  
379 for both lake basins, except for the lower-than-expected value of  $\alpha_2$  (0.984) in the  $Z_2$  of Lake  
380 Bédard. Note that  $\alpha_3$  is not given in Table 3 since the modeling of the  $\delta^{13}\text{C}$  profiles of  $\text{CH}_4$  and  
381 DIC indicates that  $R_3 = 0$  (see section S2.2.2.1 in the SI). Optimal values for  $\alpha_4$ ,  $\alpha_5$  and  $f\text{-CH}_4$  for  
382 both lake basins were also similar to those reported in our previous study on Lake Tantaré Basin  
383 B (Clayer et al., 2018).



384 Figure 3 : Comparison of the simulated (lines) and measured average ( $n = 3$ )  $\delta^{13}\text{C}$  profiles of  $\text{CH}_4$  (circles) and DIC  
 385 (squares) in the porewater of Lake Tantaré Basin A (a) and Lake Bédard (b). The horizontal dotted line indicates the  
 386 sediment-water interface. The variability in  $\delta^{13}\text{C}$  values ( $\pm$  one standard deviation –  $\sigma$ ) related to the spatial heterogeneity  
 387 within the sampling area is shown by the grey area fills. The zone  $Z_2$  is delimited by the blue area fill. In panel b, the blue  
 388 lines are the profiles simulated with the default rate values and optimal  $\alpha_1$  and  $f$  values as described in section S2.2.1. The  
 389 red lines in panel (b) are the profiles simulated with  $\alpha_2$  values of 0.980–0.984 (see section 4.1 for details).

390 **Table 3: Molecular diffusivity ratio of CH<sub>4</sub> (f-CH<sub>4</sub>) as well as the isotopic fractionation factors ( $\alpha_1$ ,  $\alpha_2$ ,  $\alpha_4$ - $\alpha_7$ ) and rates**  
 391 **(R<sub>1</sub>, R<sub>2</sub>, R<sub>4</sub>-R<sub>7</sub>; fmol cm<sup>-3</sup> s<sup>-1</sup>) of each reaction involved in OM mineralization in each zone and for the whole sediment**  
 392 **column ( $\Sigma R_i$ ; fmol cm<sup>-2</sup> s<sup>-1</sup>) corresponding to the lowest values of N<sub>res</sub>. At both study sites, R<sub>3</sub> was shown to be negligible.**  
 393 **See section S2 of the SI for details.**

Study site	Zones	f-CH <sub>4</sub>	$\alpha_1$	$\alpha_2$	$\alpha_4$	$\alpha_5$	$\alpha_6$	$\alpha_7$	R <sub>1</sub>	R <sub>2</sub>	R <sub>4</sub>	R <sub>5</sub>	R <sub>6</sub>	R <sub>7</sub>
Tantaré Basin A	Z <sub>1</sub>	1.003	1.000	-	1.094	1.024	1.000	-	132	-	119	126	84	-
	Z <sub>2</sub>	1.003	1.000	-	1.087	1.005	1.000	-	126	-	78	39	26	-
	Z <sub>3</sub>	1.003	-	-	1.085	-	-	-	-	-	1	-	-	-
	$\Sigma R_i$								931	-	721	592	394	-
Bédard	Z <sub>1</sub>	1.003	1.000	-	1.074	-	-	-	165	-	100	-	-	-
	Z <sub>2</sub>	1.003	-	0.984 <sup>a</sup>	1.074	-	-	-	72 <sup>b</sup>	145 <sup>b</sup>	50	-	-	-
	Z <sub>3</sub>	1.003	-	-	1.074	-	-	0.995	-	-	5	-	-	8
	$\Sigma R_i$								853	522	612	-	-	114

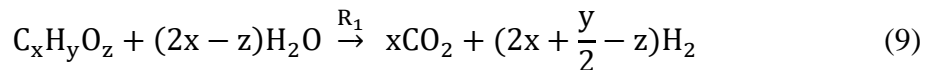
394 <sup>a</sup>the optimal value of  $\alpha_2$ , given here is for a COS value of -1.5, varies slightly with the COS value (see section  
 395 S2.2.2.3 of the SI).

396 <sup>b</sup>the value of R<sub>1</sub> and R<sub>2</sub>, given here is for a COS value of -1.5, varies with the COS value (see section S2.2.2.3 of the  
 397 SI).

## 398 4 Discussion

### 399 4.1 Organic matter mineralization pathways at the sampling sites

400 The porewater data as well as the combined modeling of carbon isotopes and  
 401 concentration profiles, allows to highlight key OM mineralization mechanisms and to quantify  
 402 the relative contribution of methanogenesis and fermentation to OM degradation at both  
 403 sampling sites The <sup>13</sup>C isotopic signatures, i.e., highly negative values of  $\delta^{13}\text{C-CH}_4$  and large  
 404 differences between  $\delta^{13}\text{C-CO}_2$  and  $\delta^{13}\text{C-CH}_4$  (section 3.3 and Fig. S2 in the SI), as well as the  
 405 modeling of the  $\delta^{13}\text{C-CO}_2$  and  $\delta^{13}\text{C-CH}_4$  profiles (section S2.2.2.1 and Fig S4a and b in the SI)  
 406 all point to hydrogenotrophy as being the only pathway for methanogenesis in the two lake  
 407 basins. The dominance of hydrogenotrophy is consistent also with the finding that acetate  
 408 concentrations were close to or below DL in the porewater samples. Under the condition that  
 409 acetocalsty is negligible (i.e.,  $x = v_1$ ), reaction r1 from Table 1 becomes:



410 Methanogenesis was also reported to be essentially hydrogenotrophic in the sediments of  
 411 Basin B of Lake Tantaré (Clayer et al 2018). The absence of acetoclasty in the sediments of the  
 412 oligotrophic lakes Bédard and Tantaré is consistent with the consensus that hydrogenotrophy  
 413 becomes an increasingly important CH<sub>4</sub> production pathway: i) when labile OM is depleted

414 (Whiticar et al., 1986; Chasar et al., 2000; Hornibrook et al., 2000), ii) with increasing  
415 sediment/soil depth (Hornibrook et al., 1997; Conrad et al., 2009), or iii) with decreasing rates of  
416 primary production in aquatic environments (Wand et al., 2006; Galand et al., 2010).

417 The modelling of concentrations and  $\delta^{13}\text{C}$  profiles revealed that oxidative processes  
418 occurred essentially in the upper 7 cm of the sediments of the perennially oxygenated Lake  
419 Tantaré Basin A, i.e., mainly in the  $Z_1$  and, to a lesser extent, in the  $Z_2$  (Table 3 and sections  
420 S2.1.2.1 and S2.1.2.2 of the SI). Moreover, it showed that methanotrophy was the dominant  
421 oxidative reaction in these sediment layers since 75% of the oxidants were consumed through r5  
422 (section S2.2.2.2 of the SI). This outcome is consistent with several studies showing that  
423 methanotrophy occurs at higher rates than OM oxidation at low EA concentrations (Sivan et al.,  
424 2007; Pohlman et al., 2013; Kankaala et al., 2013; Thottahil et al., 2019). Methanotrophy is also  
425 evidenced in the  $Z_1$  of this lake basin by the negative  $R_{\text{net}}^{\text{CH}_4}$  value and by a shift of the  $\delta^{13}\text{C}\text{-CH}_4$   
426 profiles to more positive values in their upper part (Fig. 2b and g). Use of Eq. 2 to model the EAs  
427 profiles with the code PROFILE predicts that  $\text{O}_2$  was by far the main EA involved either  
428 directly, or indirectly via the coupling with the Fe or S cycles, in the oxidative processes. Indeed,  
429 comparing the values of  $R_{\text{net}}^{\text{O}_2}$  and  $R_{\text{net}}^{\text{Ox}}$  (see Section 3.2 and Table 2) shows that  $\text{O}_2$  accounts for  
430 87% and 70% of the oxidants consumed in the  $Z_1$  and  $Z_2$  of Lake Tantaré Basin A, respectively.  
431 Since  $\text{O}_2$  penetration in the sediment by molecular diffusion is limited to  $\sim 4\text{-mm}$ , a significant  
432 amount of  $\text{O}_2$  is predicted by Eq. 2 to be transported deeper in the sediment through bioirrigation.  
433 The predominance of  $\text{O}_2$  among the EAs consumed in the sediments is consistent with our  
434 previous study in this basin of Lake Tantaré (Clayer et al., 2016). Given that methanotrophy is  
435 the dominant oxidative process and that  $\text{O}_2$  is the main oxidant consumed, it is probable that  
436 aerobic oxidation of methane prevails over its anaerobic counterpart in this lake basin. This is in  
437 line with the common thinking that  $\text{CH}_4$  oxidation in freshwater lake sediments is carried out by  
438 methanotrophs essentially in the uppermost oxic sediment layer (Bastviken et al., 2008 and  
439 references therein).

440 The sharp upward depletion in  $^{13}\text{C}\text{-CH}_4$  leading to a minimum  $\delta^{13}\text{C}\text{-CH}_4$  value at 2.5 cm  
441 depth in Lake Tantaré Basin A sediments (Fig. 3a) was unanticipated since, according to the  
442 modeling with the code PROFILE, it occurs in the methanotrophic zone, i.e., where the  
443 remaining  $\text{CH}_4$  is expected to be  $^{13}\text{C}$ -enriched as a result of  $\text{CH}_4$  oxidation. Marked  $^{13}\text{C}\text{-CH}_4$

444 depletions at the base of the sulfate-methane transition zone, where  $\text{CH}_4$  is consumed via  $\text{SO}_4^{2-}$   
 445 reduction, have often been observed in marine sediments (Burdige et al., 2016 and references  
 446 therein). Such features are generally attributed to the production of  $\text{CH}_4$  by hydrogenotrophy  
 447 from the  $^{13}\text{C}$ -depleted DIC resulting from the anaerobic  $\text{CH}_4$  oxidation, a process referred to as  
 448 intertwined methanotrophy and hydrogenotrophy (e.g., Borowski et al., 1997; Pohlman et al.,  
 449 2008; Burdige et al., 2016). Here the modelled  $\delta^{13}\text{C}$ - $\text{CH}_4$  profile captured the minimum in  $\delta^{13}\text{C}$ -  
 450  $\text{CH}_4$  in the  $Z_1$  by simply assuming concomitant hydrogenotrophy and methanotrophy in this zone  
 451 and an upward-increasing  $\alpha_4$  value from 1.085 in the  $Z_3$  to 1.094 in the  $Z_1$  (section S2.2.1 of the  
 452 SI). These  $\alpha_4$  values remain within the range reported for this isotope fractionation factor (Table  
 453 S1 in the SI). A small variation with sediment depth in the fractionation factor  $\alpha_4$  is arguably  
 454 possible since its value depends on the types of microorganisms producing  $\text{CH}_4$  (Conrad 2005).  
 455 The possibility that a depth variation in this isotope fractionation factor could explain some of  
 456 the minima in  $\delta^{13}\text{C}$ - $\text{CH}_4$  reported in other studies should be considered.

457 In the  $Z_2$  of Lake Bédard, the net rate of DIC production (i.e.,  $167 \text{ fmol cm}^{-3} \text{ s}^{-1}$ ) was  
 458 more than 3 times that of  $\text{CH}_4$  production ( $50 \text{ fmol cm}^{-3} \text{ s}^{-1}$ ; Table 2). Given that the  $R_{\text{net}}^{\text{Ox}}$  was  
 459 negligible in this zone (i.e.,  $R_5 = R_6 = 0$ ), we obtain from Eqs 3 and 4 and Table 2 that  $R_{\text{net}}^{\text{CH}_4} =$   
 460  $R_4 = 50 \text{ fmol cm}^{-3} \text{ s}^{-1}$  and  $R_{\text{net}}^{\text{DIC}} = R_1 + R_2 - R_4 = 167 \text{ fmol cm}^{-3} \text{ s}^{-1}$  (see section S2.1.2.2  
 461 of the SI). Should we assume that DIC production by r2 is negligible, i.e.,  $R_2 = 0$ , a  $R_1/R_4$  ratio of  
 462 4.3 would be obtained. This high ratio indicates that DIC was not produced by hydrogenotrophy  
 463 (r4) coupled to fermentation (r1) alone in the  $Z_2$  of this lake. Indeed, methanogenesis through the  
 464 coupling of these two reactions yields a  $R_1/R_4$  ratio of 2 if the fermenting substrate is  
 465 carbohydrates (COS of 0) and lower than 2 if the fermenting substrate has a negative COS value.  
 466 We thus attributed the production of the additional DIC to the partial fermentation of HMW OM,  
 467 an assumed non-fractionating process reported to occur in wetlands (Corbett et al., 2015). The  
 468 better fitting of the  $\delta^{13}\text{C}$ -DIC profile when  $\alpha_2$  is set to 0.980–0.984 rather than to 1.000 in the  $Z_2$   
 469 (compare the blue and red lines in Fig. 4b) suggests that C fractionates during this partial  
 470 fermentation process.

471 Table 3 displays the depth-integrated reaction rates ( $\Sigma R_i$ ) over the top 21cm of the  
 472 sediment column which are given by:

$$\Sigma R_i = \sum_{j=1}^3 \Delta x_j R_i \quad (10)$$

473 where  $\Delta x_j$  (cm) is the thickness of the zone  $Z_j$ . In this calculation, we assume that other zones of  
 474  $\text{CH}_4$  or DIC production are absent below 21 cm. Values of  $\Sigma R_i$  clearly show that anaerobic  
 475 carbon mineralization reactions (fermentation and methanogenesis) are important contributors to  
 476 the overall OM mineralization in the two studied lake basins. Indeed, the sum of the rates of  $\text{CH}_4$   
 477 production ( $\Sigma R_4$ ), DIC production due to  $\text{CH}_4$  formation ( $\Sigma R_1 - \Sigma R_4$ ) and HMW OM partial  
 478 fermentation ( $\Sigma R_2$ ) represents 49% and 100% of the total OM degradation rate ( $\Sigma R_1 + \Sigma R_2 + \Sigma R_5$   
 479  $+ \Sigma R_6$ ) in the sediment of lakes Tantaré Basin A and Bédard, respectively. The contribution of  
 480 anaerobic mineralization for Lake Tantaré Basin A is about 1.6 times higher than the average of  
 481 30% reported for this lake basin in a previous study (Clayer et al., 2016). This significant  
 482 discrepancy arises because these authors, in the absence of isotopic data to adequately constrain  
 483 the  $R_i$  values, assumed that  $R_4 = 0$  in the net methanotrophic zone  $Z_1$ . Should we make the same  
 484 assumption in the present study, we would also estimate that fermentation and methanogenesis  
 485 represent only 30% of the total rate of OM degradation in the oxygenated Lake Tantaré Basin A  
 486 and we would thus underestimate the importance of methanogenesis. The inclusion of  $\delta^{13}\text{C}$  data  
 487 in the present modeling study thus allowed to better constrain the effective rates of  $\text{CH}_4$   
 488 production ( $R_4$ ).

#### 489 4.2 Organic substrates for methanogenesis at the sampling sites

490 Table 3 indicates that hydrogenotrophy ( $r_4$ ) coupled to the complete fermentation of OM  
 491 ( $r_1$ ) produces  $\text{CH}_4$  at higher rates ( $R_4$ ) than DIC ( $R_1 - R_4$ ) in the  $Z_1$  and  $Z_2$  of both lake basins.  
 492 This outcome is inconsistent with the equimolar production of  $\text{CH}_4$  and DIC expected from the  
 493 fermentation of glucose ( $\text{C}_6\text{H}_{12}\text{O}_6$ ), the model molecule used to represent labile OM in diagenetic  
 494 models (Paraska et al., 2014), thus suggesting that the fermentation of this compound is not the  
 495 exclusive source of the  $\text{H}_2$  required for hydrogenotrophy. Had OM been represented by  $\text{C}_6\text{H}_{12}\text{O}_6$   
 496 in  $r_1$ , the rate of  $\text{H}_2$  production by this reaction would have been twice that of  $\text{CO}_2$ , i.e.,  $2R_1$ . For  
 497 its part, the rate of  $\text{H}_2$  consumption through hydrogenotrophy is four times that of the  $\text{CH}_4$   
 498 production, i.e.,  $4R_4$ . Hence, an additional  $\text{H}_2$  production at rates of up to 212 and 70  $\text{fmol cm}^{-3}$   
 499  $\text{s}^{-1}$ , i.e.,  $4R_4 - 2R_1$ , is needed to balance the  $\text{H}_2$  production rate expected from the fermentation

500 of  $C_6H_{12}O_6$  and the  $H_2$  consumption rate by hydrogenotrophy observed in the sediments of Lake  
 501 Tantaré Basin A and Lake Bédard, respectively. As discussed by Clayer et al. (2018), this  
 502 additional production rate of  $H_2$  could be provided by a cryptic Fe-S cycle such as r8 (Table 1), or  
 503 by the production of  $CH_4$  via the fermentation of organic substrates more reduced than glucose.

504 The progressive downward increases in dissolved Fe and  $SO_4^{2-}$  (Fig. 2e, f, m and n)  
 505 below  $\sim 5$  cm depth and decrease in  $\Sigma S(-II)$  (Fig. 2n) observed in the porewaters support a  
 506 production of  $H_2$  from r8 in both lakes. However, modeling the appropriate solute profiles with  
 507 the code PROFILE indicates that the production rates of dissolved Fe ( $< 10 \text{ fmol cm}^{-3} \text{ s}^{-1}$ ) and  
 508  $SO_4^{2-}$  ( $< 1 \text{ fmol cm}^{-3} \text{ s}^{-1}$ ) and the consumption rate of  $\Sigma S(-II)$  ( $< 1 \text{ fmol cm}^{-3} \text{ s}^{-1}$ ) are about one  
 509 order of magnitude too low to explain the missing  $H_2$  production rate in both basins. Moreover,  
 510 in the  $Z_1$  and  $Z_2$  of Lake Tantaré Basin A, the rate of solid Fe(III) reduction ( $< 3 \text{ fmol cm}^{-3} \text{ s}^{-1}$ ;  
 511 calculated from Liu et al. 2015) is much lower than that required from r8 (i.e., 1 to 2 times the  
 512 additional  $H_2$  production of  $4R_4 - 2R_1$ ;  $70\text{--}424 \text{ fmol cm}^{-3} \text{ s}^{-1}$ ) to produce sufficient amounts of  
 513  $H_2$  to sustain the additional hydrogenotrophy. Given these results, we submit that a cryptic Fe-S  
 514 cycle, if present, would contribute only minimally to the missing rate of  $H_2$  production, and that  
 515 the fermentation of reduced organic compounds could provide a better explanation to the  
 516 imbalance between the  $H_2$  production and consumption rates.

517 Since  $CH_4$  is produced by hydrogenotrophy in the two lake basins ( $\chi_H = 1$ ), Eqn. S15  
 518 (section S2.2.2. of the SI) describing the COS of the fermenting organic substrate  $C_xH_yO_z$   
 519 simplifies as:

$$\text{COS} = -4 \left( \frac{2 \left( R_{\text{net}}^{\text{CH}_4} - \frac{1}{2} \chi_M R_{\text{net}}^{\text{Ox}} \right) - R_1}{R_1} \right) \quad (11)$$

520 where  $\chi_M$  is the fraction of oxidants consumed through methanotrophy. Combining Eqs. S7 and  
 521 S5 of the SI with Eq. 11, we obtain:

$$\text{COS} = -4 \left( \frac{R_{\text{net}}^{\text{CH}_4} - R_{\text{net}}^{\text{DIC}} - R_{\text{net}}^{\text{Ox}} + R_2}{R_{\text{net}}^{\text{DIC}} + R_{\text{net}}^{\text{CH}_4} + (1 - \chi_M) R_{\text{net}}^{\text{Ox}} - R_2} \right) \quad (12)$$

522 Introducing the values of  $R_{\text{net}}^{\text{CH}_4}$ ,  $R_{\text{net}}^{\text{DIC}}$ ,  $R_{\text{net}}^{\text{Ox}}$  and  $R_2$  (Table 2 and 3) into Eq. 12, we  
 523 calculate COS values of  $-3.2$  and  $-0.9$  for the  $Z_1$  and  $Z_2$  of Lake Tantaré Basin A, respectively,

524 and of  $-1.0$  to  $-1.1$  for the  $Z_1$  of Lake Bédard, respectively. Note that we were unable to  
525 constrain with Eq. 12 the COS for the  $Z_2$  of Lake Bédard since we had to assume a COS value to  
526 estimate  $R_2$  and the COS has no influence of the modelled  $\delta^{13}\text{C}$  profiles (section S2.2.2.3 of the  
527 SI). Negative COS values between  $-0.9$  and  $-1.1$  suggest that fermenting OM in the sediments  
528 of the two lake basins would be better represented by a mixture of fatty acids and fatty alcohols  
529 than by carbohydrates, as suggested by Clayer et al. (2018) for the sporadically anoxic Lake  
530 Tantaré Basin B. For its part, the highly negative COS value of  $-3.2$  calculated for the  $Z_1$  of  
531 Lake Tantaré Basin A is unreasonable, and the inaccuracy of the COS determination in this lake  
532 basin is discussed in section 4.3.

#### 533 4.3 Reduced organic compounds as methanogenic substrates in lake sediments

534 In order to better appraise the COS of the fermenting OM in lakes, relevant datasets of  
535 porewater solute concentration profiles were gathered from our data repository and from a  
536 thorough literature search. To be able to obtain by reactive-transport modeling the  $R_{\text{net}}^{\text{solute}}$   
537 required to calculate the COS with Eq. 12, the datasets had to: (i) comprise porewater  
538 concentration profiles of  $\text{CH}_4$  and DIC and, ideally, those of the EAs; (ii) reveal a net  
539 methanogenesis zone, and (iii) enable the carbonate precipitation/dissolution contribution to the  
540 DIC concentrations to be estimated. Detailed information on the origin and processing of the 17  
541 selected datasets, acquired in 6 different lake basins from one sub-alpine and three boreal lakes  
542 sampled at various dates and/or depths, is given in section S3 of the SI. The  $\text{CH}_4$  and DIC  
543 porewater profiles determined at hypolimnetic sites of these lake basins and their modeling with  
544 the code PROFILE are shown in Fig. 4, whereas the  $R_{\text{net}}^{\text{CH}_4}$ ,  $R_{\text{net}}^{\text{DIC}}$  and  $R_{\text{net}}^{\text{Ox}}$  values determined  
545 from this modeling are regrouped in Table 4. The COS values displayed in Table 4 for all lake  
546 basins and dates were calculated by substituting the appropriate  $R_{\text{net}}^{\text{CH}_4}$ ,  $R_{\text{net}}^{\text{DIC}}$  and  $R_{\text{net}}^{\text{Ox}}$  values in  
547 Eq. 12 and assuming that  $R_2 = 0$ . This latter assumption was not required Lake Tantaré Basin A  
548 (October 2015) and Lake Bédard (October 2015) for which  $R_2$  values were known (Table 4).  
549 Equation 12 indicates that any DIC contribution from  $r_2$  would yield lower COS values than  
550 those reported in Table 4. The value of  $\chi_M$  was assumed to be alternately 0 and 1 to provide a  
551 range of COS values. The only exception was Lake Tantaré Basin A in October 2015 for which  
552  $\chi_M$  is known to be 0.75 (section S2.2.2.2 of the SI). Note that although Eq. 12 was derived with

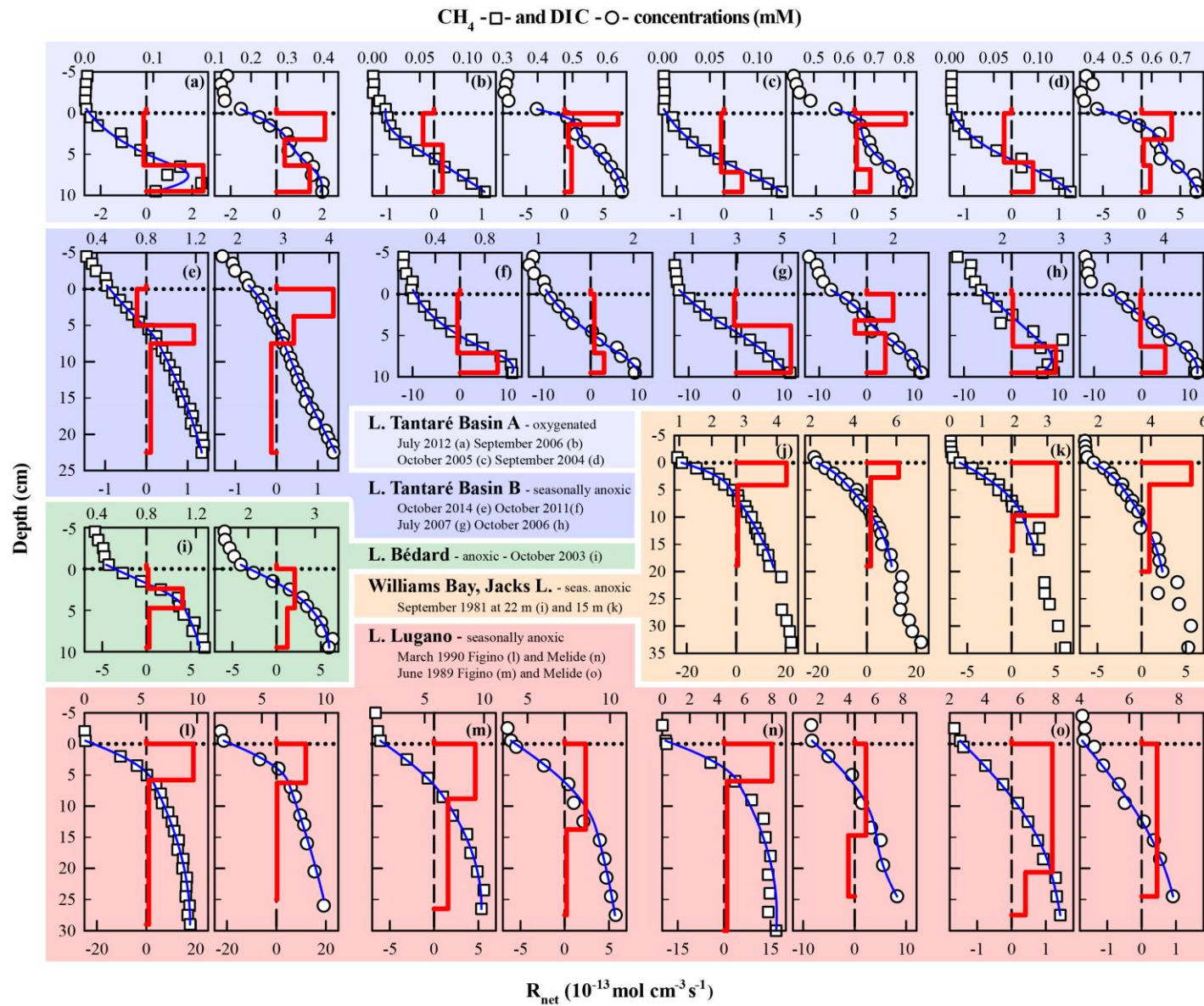
553 the assumption that methanogenesis was hydrogenotrophic ( $\chi_H = 1$ ), assuming that  $\text{CH}_4$  was  
 554 produced by acetoclasty ( $\chi_H = 0$ ) would yield the same expression.

555 **Table 4: Net reaction rates ( $R_{\text{net}}^{\text{solute}}$ ;  $\text{fmol cm}^{-3} \text{s}^{-1}$ ) of  $\text{CH}_4$ , DIC and oxidants in the zone with the highest production rate  
 556 of  $\text{CH}_4$  as well as the  $\text{O}_2$  concentration in the bottom water ( $[\text{O}_2]$  in  $\text{mg L}^{-1}$ ), the  $R_2$  rates ( $\text{fmol cm}^{-3} \text{s}^{-1}$ ) and the average  
 557 carbon oxidation state (COS) of the fermenting OM at the origin of  $\text{CH}_4$  calculated with Eq. (12) at both study sites, Lake  
 558 Tantaré Basin B (Fig. 1), Jacks Lake (Carignan and Lean 1991) and Lake Lugano (Lazzaretti-Ulmer & Hanselmann  
 559 1999) for various sampling dates.**

Lake Basin	Sampling date	$[\text{O}_2]$	$R_{\text{net}}^{\text{DIC}}$	$R_{\text{net}}^{\text{CH}_4}$	$R_{\text{net}}^{\text{Ox}}$	$R_2$	Reference	COS <sup>a</sup>	
								Min.	Max.
Tantaré Basin A, 15 m	Oct 2015 – Z <sub>1</sub>	3.5	223	-7	-335	0	this study	-3.2	-3.2
	Oct 2015 – Z <sub>2</sub>	3.5	113	39	-103	0	this study	-0.9	-0.9
	Jul 2012	6.0	143	245	-66	-	1	-2.1	-1.7
	Sep 2006	4.0	89	33	-45	-	1	0.4	0.6
	Oct 2005	3.1	202	48	-44	-	1	1.8	2.1
	Sep 2004	4.6	99	45	-60	-	1	-0.3	-0.2
Tantaré Basin B, 22 m	Oct 2014	< 0.1	42	116	-1	-	2	-1.9	-1.9
	Oct 2011	0.4	279	783	-12	-	1	-2.0	-1.9
	Jul 2007	4.1	283	1147	-20	-	1	-2.5	-2.5
	Oct 2006	< 0.1	442	825	-2	-	1	-1.2	-1.2
Bédard, 10 m	Oct 2015 – Z <sub>1</sub>	< 0.1	65	100	-6.5	0	this study	-1.1	-1.0
	Oct 2003	< 0.1	205	408	-13	-	3	-1.4	-1.4
Jacks Lake, 15 m	Sep 1981	na	284	514	-	-	4	-1.2	-1.2
Jacks Lake, 22 m	Sep 1981	na	904	2030	-	-	4	-1.5	-1.5
Lugano, Melide, 85 m	Mar 1989	2.0	228	388	-83	-	5	-1.8	-1.6
Lugano, Melide, 85 m	Jun 1989	< 0.1	45	97	-1	-	5	-1.5	-1.5
Lugano, Figino, 95 m	Mar 1989	4.0	1168	1903	-234	-	5	-1.4	-1.3
Lugano, Figino, 95 m	Jun 1989	< 0.1	237	355	-19	-	5	-1.0	-0.9

560 <sup>a</sup> Minimum and Maximum COS values were obtained by setting  $\chi_M$  to 0 and 1 in Eq. (12), except for Tantaré Basin  
 561 A in October 2015 for which  $\chi_M$  is known to be 0.75.

562 References: (1) Clayer et al. (2016), (2) Clayer et al. (2018), (3) see Supporting Information, (4) Carignan and Lean  
 563 (1991), (5) Lazzaretti-Ulmer & Hanselmann (1999).



564 Figure 4 : Comparison of the modeled (blue lines) and average ( $n = 3$ ) measured concentration profiles of  $\text{CH}_4$  (squares) and DIC (circles) in Lakes Tantaré Basin A (a–  
 565 d) and Basin B (a–h), Bédard (i), Jacks Lake (j–k) and Lake Lugano (l–o) at various sampling dates. The thick red lines represent the net solute reaction rate ( $R_{\text{net}}^{\text{solute}}$ ).

566 According to Table 4 the COS values are systematically negative at all dates for Lake  
567 Tantaré Basin B, Lake Bédard, Jacks Lake and the two sites of Lake Lugano, and they vary  
568 generally between  $-0.9$  and  $-1.9$ , with the exception of a value of  $-2.5$  obtained for Lake  
569 Tantaré Basin B in July 2007. This latter value is likely too low to be representative of  
570 fermenting material and should be rejected. The mean ( $\pm$  SD) COS values are  $-1.7 \pm 0.4$  for  
571 Lake Tantaré Basin B,  $-1.4 \pm 0.4$  for Lake Bédard,  $-1.4 \pm 0.2$  for Jacks Lake and  $-1.4 \pm 0.3$  for  
572 Lake Lugano. These COS values, representative of a mixture of fatty acids (COS of  $-1.0$  for C4-  
573 fatty acids to about  $-1.87$  for C32-fatty acids) and of fatty alcohols (COS =  $-2.00$ ), strongly  
574 supports the idea that methanogenesis in boreal lakes sediments, as well as in the sediments of  
575 other types of lakes, is fueled by more reduced organic compounds than glucose. Lipids such as  
576 fatty acids and fatty alcohols with similar COS are naturally abundant in sediments to sustain the  
577 estimated rates of  $\text{CH}_4$  and DIC production during fermentation (Hedges and Oades, 1997;  
578 Cranwell, 1981; Matsumoto, 1989; Burdige, 2006). As discussed by Clayer et al. (2018) the most  
579 labile organic compounds (i.e., proteins and carbohydrates) can be rapidly degraded during their  
580 transport through the water column and in the uppermost sediment layer, leaving mainly lipids as  
581 metabolizable substrates at depths where fermentation and methanogenesis occurs. This  
582 interpretation is consistent with thermodynamic and kinetic evidences that proteins and  
583 carbohydrates are more labile and are degraded faster than lipids (LaRowe and Van Cappellen,  
584 2011).

585 The COS values determined for the perennially oxygenated Basin A of Lake Tantaré  
586 (mean of  $-0.6 \pm 1.1$ ; range of  $-3.2$  to  $2.1$ ; Table 4) are much more variable than for the five other  
587 lake basins which undergo seasonal anoxia. Moreover, the COS values estimated for October  
588 2015 in the  $Z_1$  ( $-3.2$ ), September 2016 ( $0.4$ – $0.6$ ) and October 2005 ( $1.8$ – $2.1$ ) are unrealistic.  
589 Indeed, the very negative value of  $-3.2$  does not correspond to any degradable compound under  
590 anoxic conditions, whereas the positive values of  $0.4$ – $0.6$  and  $1.8$ – $2.1$  would involve either  
591 amino acids and nucleotides which are very labile (Larowe and Van Cappellen 2011) and tend to  
592 be degraded in the water column (Burdige 2007) or oxidized compounds, such as ketones,  
593 aldehydes and esters, known to be quickly reduced to alcohols. These observations indicate that  
594 the COS determination in this lake basin is unreliable. The misestimation of the COS can  
595 probably not be explained by the presence of  $\text{O}_2$  itself at the sediment surface of Lake Tantaré  
596 Basin A. Indeed, the sediment surface was also oxic at the sites Melide and Figino of Lake

597 Lugano in March 1989 (Table 4) as revealed by detectable bottom water [O<sub>2</sub>] (Table 4), and by  
598 low [Fe], undetectable ΣS(-II) and [CH<sub>4</sub>] and relatively high [SO<sub>4</sub><sup>2-</sup>] in overlying water  
599 (Lazzaretti et al., 1992; Lazzaretti-Ulmer and Hanselmann, 1999). Despite this, the COS values  
600 determined for the two sites of Lake Lugano appear to be realistic and coherent with those  
601 calculated for Lakes Tantaré Basin B, Bédard and Jacks. However, we know that benthic  
602 organisms are present in Lake Tantaré Basin A (Hare et al., 1994) but lacking at the two sites of  
603 Lake Lugano, as shown by the presence of varves (Span et al., 1992) and the absence of benthos  
604 remains in the recent sediments at these sites (Niessen et al., 1992). Clayer et al. (2016) provided  
605 evidences that sediment irrigation by benthic animals is effective in Lake Tantaré Basin A and  
606 that it should be taken into account in modeling the porewater solutes profiles. However, these  
607 authors also point out the difficulty to properly estimate the magnitude of solute transport by  
608 bioirrigation. The term used in Eq. 2 to calculate this contribution, i.e.,  $\varphi\alpha_{\text{irrigation}} ([\text{solute}]_{\text{tube}} -$   
609  $[\text{solute}])$ , is indeed an approximation of intricate 3-D processes (Meile et al. 2005). And, in the  
610 conceptualization of this bioirrigation term, it was notably assumed that benthic animals  
611 continuously irrigate their tubes to maintain solute concentrations in their biogenic structures  
612 ( $[\text{solute}]_{\text{tube}}$ ) identical to those in the water overlying the sediments. But microbenthic animals  
613 are generally reported to irrigate the sediments in a discontinuous manner and the solute  
614 concentrations in their biogenic structures may be highly variable with time (Boudreau and  
615 Marinelli 1994; Forster and Graf 1995; Riisgård and Larsen 2005; Gallon et al. 2008). Hence,  
616 owing to the imperfection of the representation of bioirrigation in Eq. 2, COS values estimated  
617 for the sediment of Lake Tantaré Basin A should be treated with caution, especially in the Z<sub>1</sub>  
618 where the bioirrigation coefficient takes the highest value. Another potential bias in the  
619 estimation of COS values for the oxygenated basin is the possibility of DIC production through  
620 HMW OM fermentation (reaction r<sub>2</sub>; Corbett et al. 2013). Note that fitting with Eq. 6 the  
621 experimental δ<sup>13</sup>C data does not allow partitioning the production of DIC between r<sub>1</sub> and r<sub>2</sub>  
622 since the two processes share the same value of fractionation factor ( $\alpha_1 = \alpha_2 = 1.000$ ). It was  
623 possible to attribute unequivocally the excess of DIC production rate over that of CH<sub>4</sub> production  
624 in the Z<sub>2</sub> of Lake Bédard in October 2015 (Table 4 and Section S2.1.2.2 of the SI) to HMW OM  
625 fermentation merely because  $R_{\text{net}}^{\text{Ox}}$  was negligible compared to  $R_{\text{net}}^{\text{CH}_4}$  and  $R_{\text{net}}^{\text{DIC}}$ , which is not the  
626 case for Lake Tantaré Basin A (Table 4). Equation 12 indicates that to obtain negative COS  
627 values for Lake Tantaré Basin A in September 2006 and October 2005, R<sub>2</sub> should be >11 fmol

628  $\text{cm}^{-2} \text{s}^{-1}$  and  $>110 \text{ fmol cm}^{-2} \text{ s}^{-1}$ , respectively. These  $R_2$  values correspond to transferring  $>9\%$   
629 and  $>44\%$  of the rate of DIC production from  $R_1$  to  $R_2$  for September 2006 and October 2005,  
630 respectively. The above discussion underlines several factors that can explain the unreliability in  
631 the actual COS estimation for the perennially oxic Lake Tantaré Basin A, and further research is  
632 needed to better assess the importance of these factors. However, it does not dismiss that the  
633 substrate for methanogenesis in this lake basin may have a negative COS value.

## 634 **5 Conclusions**

635 Our results show that fermentation and methanogenesis represent nearly 50% and 100%  
636 of OM mineralization in the top 25 cm of the sediments at the hypolimnetic sites in Lake Bédard  
637 and in Basin A of Lake Tantaré, respectively and that methane is produced only by  
638 hydrogenotrophy at these two sites. An earlier study reached similar conclusions about the  
639 pathways of methanogenesis and the contribution of this process in OM mineralization in Basin  
640 B of Lake Tantaré (Clayer et al. 2018).

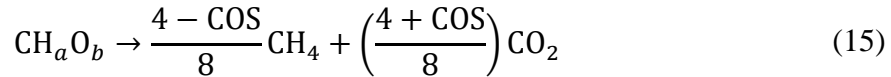
641 Reactive-transport modelling of porewater solutes from three boreal lakes, i.e., Bédard,  
642 Tantaré (Basin B) and Jacks, as well as of the sub-alpine Lake Lugano (Melide and Figino sites)  
643 consistently showed that the main substrates for sediment methanogenesis at deep seasonally  
644 anoxic hypolimnetic sites have a mean COS value of  $-1.4 \pm 0.3$ . Mineralization of the most  
645 labile compounds during OM downward migration in the water column and in the uppermost  
646 sediment layers likely explains why reduced organic compounds fuel methanogenesis in these  
647 sediments.

648 The current representation of the fermenting OM, i.e.,  $\text{CH}_2\text{O}$ , in process-based  
649 biogeochemical models entails a significant risk of misestimating sedimentary  $\text{CH}_4$  and  $\text{CO}_2$   
650 production and release to the bottom water and, to a certain extent, of mispredicting evasion of  
651 these greenhouse gases to the atmosphere under transient environmental scenarios. To better  
652 constrain  $\text{CH}_4$  and  $\text{CO}_2$  production within sediments, we suggest taking specifically into account  
653 the COS of the fermenting OM in formulating the reactions of methanogenesis associated with  
654 fermentation in these models. For example, the rates of  $\text{CH}_4$  ( $R^{\text{CH}_4}$ ) and DIC ( $R^{\text{DIC}}$ ) production  
655 during fermentation coupled to hydrogenotrophy can be expressed as:

$$R^{\text{CH}_4} = R_4 = \frac{4 - \text{COS}}{8} R_1 \quad (13)$$

$$R^{\text{DIC}} = R_1 - R_4 = R_1 \left( 1 - \frac{4 - \text{COS}}{8} \right) \quad (14)$$

656 Given these rate expressions, the stoichiometric formulation of a typical fermentation  
657 reaction producing methane becomes:



658 where  $a = 2 - \frac{\text{COS}}{2}$ ,  $b = 1 + \frac{\text{COS}}{4}$ . Note that the same stoichiometric formulation would be  
659 obtained for acetoclastic methanogenesis.

660 The approach used to estimate the COS of the fermenting OM, although successful for  
661 the seasonally anoxic basins, failed to produce reliable COS values when applied to the  
662 perennially oxygenated Basin A of Lake Tantaré. We attribute this peculiarity to a misestimation  
663 and/or misrepresentation of the benthic irrigation and to the impossibility to partition the DIC  
664 production between reactions r1 and r2 which share the same fractionation factor value. Similar  
665 problems would likely be encountered also in other lake ecosystems such as epilimnetic  
666 sediments and wetlands where solute transport processes remain ill-known. Indeed, these  
667 shallow aquatic environments are subject to enhanced benthic activity (Hare 1995), to plant-  
668 mediated transport of CH<sub>4</sub> and O<sub>2</sub> (Chanton et al. 1989; Wang et al. 2006), as well as to  
669 turbulence (Poindexter et al. 2016) which complicates the estimation of CH<sub>4</sub> and CO<sub>2</sub> production  
670 and consumption rates. Hence, the remaining challenge resides in the robust estimations the COS  
671 of the fermenting OM in epilimnetic sediments and shallow freshwater environments (e.g.,  
672 ponds, wetlands), since these environments were shown to be the main contributors to freshwater  
673 CH<sub>4</sub> release to the atmosphere (Del Sontro et al., 2016, Bastviken et al., 2008). One potential  
674 solution is to investigate trends in the oxygen isotope signatures in the sedimentary DIC in  
675 addition to δ<sup>13</sup>C values since it is also influenced by the source of the OM undergoing  
676 degradation (e.g., Sauer et al., 2001).

677 **Acknowledgments, Samples, and Data**

678 We thank P. Boissinot, L. Rancourt, P. Girard, J.-F. Dutil, S. Duval, A. Royer-Lavallée,  
679 A. Laberge and A. Barber for research and field work assistance. We are also thankful to J.-F.  
680 Hélié, from the Laboratoire de géochimie des isotopes stables légers (UQÀM), who graciously  
681 calibrated our  $\delta^{13}\text{C}$  internal standard. This work was supported by grants to C.G., A.T. and Y.G.  
682 from the Natural Sciences and Engineering Research Council of Canada and the Fonds de  
683 Recherche Québécois – Nature et Technologies. Permission from the Québec Ministère du  
684 Développement durable, de l'Environnement et de la Lutte contre les changements climatiques  
685 to work in the Tantaré Ecological Reserve is gratefully acknowledged.

686 Data access: Upon acceptance, readers will be able to access the data at this url:

687 <https://www.hydroshare.org/resource/38e069761d7b4cf4abe3cbcaaac06016/>

688 **References**

- 689 Alperin, M. J., Albert, D. B., & Martens, C. S. (1994). Seasonal variations in production and  
690 consumption rates of dissolved organic carbon in an organic-rich coastal sediment. *Geochimica*  
691 *et Cosmochimica Acta*, 58(22), 4909–4930. [https://doi.org/10.1016/0016-7037\(94\)90221-6](https://doi.org/10.1016/0016-7037(94)90221-6)
- 692 Alperin, M. J., Reeburgh, W. S., & Whiticar, M. J. (1988). Carbon and hydrogen isotope  
693 fractionation resulting from anaerobic methane oxidation. *Global Biogeochemical Cycles*, 2(3),  
694 279–288. <https://doi.org/10.1029/GB002i003p00279>
- 695 Arndt, S., Jørgensen, B. B., LaRowe, D. E., Middelburg, J. J., Pancost, R. D., & Regnier, P.  
696 (2013). Quantifying the degradation of organic matter in marine sediments: A review and  
697 synthesis. *Earth-Science Reviews*, 123, 53–86. <https://doi.org/10.1016/j.earscirev.2013.02.008>
- 698 Arning, E. T., van Berk, W., & Schulz, H.-M. (2016). Fate and behaviour of marine organic  
699 matter during burial of anoxic sediments: Testing CH<sub>2</sub>O as generalized input parameter in  
700 reaction transport models. *Marine Chemistry*, 178, 8–21.  
701 <https://doi.org/10.1016/j.marchem.2015.12.002>
- 702 Barbieri, A., & Mosello, R. (1992). Chemistry and trophic evolution of Lake Lugano in relation  
703 to nutrient budget. *Aquatic Sciences*, 54(3), 219–237. <https://doi.org/10.1007/BF00878138>

- 704 Bastviken, D., Cole, J. J., Pace, M. L., & Van de Bogert, M. C. (2008). Fates of methane from  
705 different lake habitats: Connecting whole-lake budgets and CH<sub>4</sub> emissions. *Journal of*  
706 *Geophysical Research: Biogeosciences*, *113*(G2). <https://doi.org/10.1029/2007JG000608>
- 707 Bastviken, D., Cole, J., Pace, M., & Tranvik, L. (2004). Methane emissions from lakes:  
708 Dependence of lake characteristics, two regional assessments, and a global estimate. *Global*  
709 *Biogeochemical Cycles*, *18*(4). <https://doi.org/10.1029/2004GB002238>
- 710 Beal, E. J., House, C. H., & Orphan, V. J. (2009). Manganese- and iron-dependent marine  
711 methane oxidation. *Science (New York, N.Y.)*, *325*(5937), 184–187.  
712 <https://doi.org/10.1126/science.1169984>
- 713 Berg, P., Risgaard-Petersen, N., & Rysgaard, S. (1998). Interpretation of measured concentration  
714 profiles in sediment pore water. *Limnology and Oceanography*, *43*(7), 1500–1510.  
715 <https://doi.org/10.4319/lo.1998.43.7.1500>
- 716 Blair, N. E., & Carter, W. D. (1992). The carbon isotope biogeochemistry of acetate from a  
717 methanogenic marine sediment. *Geochimica et Cosmochimica Acta*, *56*(3), 1247–1258.  
718 [https://doi.org/10.1016/0016-7037\(92\)90060-V](https://doi.org/10.1016/0016-7037(92)90060-V)
- 719 Borowski, W. S., Paull, C. K., & Ussler, W. (1997). Carbon cycling within the upper  
720 methanogenic zone of continental rise sediments; An example from the methane-rich sediments  
721 overlying the Blake Ridge gas hydrate deposits. *Marine Chemistry*, *57*(3), 299–311.  
722 [https://doi.org/10.1016/S0304-4203\(97\)00019-4](https://doi.org/10.1016/S0304-4203(97)00019-4)
- 723 Bottinga, Y. (1969). Calculated fractionation factors for carbon and hydrogen isotope exchange  
724 in the system calcite-carbon dioxide-graphite-methane-hydrogen-water vapor. *Geochimica et*  
725 *Cosmochimica Acta*, *33*(1), 49–64. [https://doi.org/10.1016/0016-7037\(69\)90092-1](https://doi.org/10.1016/0016-7037(69)90092-1)
- 726 Boudreau, B., & Marinelli, R. (1994). A modeling study of discontinuous biological irrigation.  
727 *Journal of Marine Research*, *52*, 947–968. <https://doi.org/10.1357/0022240943076902>
- 728 Boudreau, B. P. (1997). *Diagenetic models and their implementation: modelling transport and*  
729 *reactions in aquatic sediments*. Springer.
- 730 Burdige, D. J. (2007). Preservation of Organic Matter in Marine Sediments: Controls,  
731 Mechanisms, and an Imbalance in Sediment Organic Carbon Budgets? *Chemical Reviews*,  
732 *107*(2), 467–485. <https://doi.org/10.1021/cr050347q>

- 733 Burdige, D. J., & Komada, T. (2011). Anaerobic oxidation of methane and the stoichiometry of  
734 remineralization processes in continental margin sediments. *Limnology and Oceanography*,  
735 *56*(5), 1781–1796. <https://doi.org/10.4319/lo.2011.56.5.1781>
- 736 Burdige, D., Komada, T., Magen, C., & Chanton, J. P. (2017). Methane dynamics in Santa  
737 Barbara Basin (USA) sediments as examined with a reaction-transport model. *Journal of Marine*  
738 *Research*, *74*, 277–313.
- 739 Carignan, R., & Lean, D. R. S. (1991). Regeneration of dissolved substances in a seasonally  
740 anoxic lake: The relative importance of processes occurring in the water column and in the  
741 sediments. *Limnology and Oceanography*, *36*(4), 683–707.  
742 <https://doi.org/10.4319/lo.1991.36.4.0683>
- 743 Carignan, R., Rapin, F., & Tessier, A. (1985). Sediment porewater sampling for metal analysis:  
744 A comparison of techniques. *Geochimica et Cosmochimica Acta*, *49*(11), 2493–2497.  
745 [https://doi.org/10.1016/0016-7037\(85\)90248-0](https://doi.org/10.1016/0016-7037(85)90248-0)
- 746 Carmichael, M. J., Bernhardt, E. S., Bräuer, S. L., & Smith, W. K. (2014). The role of vegetation  
747 in methane flux to the atmosphere: should vegetation be included as a distinct category in the  
748 global methane budget? *Biogeochemistry*, *119*(1), 1–24. [https://doi.org/10.1007/s10533-014-](https://doi.org/10.1007/s10533-014-9974-1)  
749 [9974-1](https://doi.org/10.1007/s10533-014-9974-1)
- 750 Chanton, J. P., Whiting, G. J., Blair, N. E., Lindau, C. W., & Bollich, P. K. (1997). Methane  
751 emission from rice: Stable isotopes, diurnal variations, and CO<sub>2</sub> exchange. *Global*  
752 *Biogeochemical Cycles*, *11*(1), 15–27. <https://doi.org/10.1029/96GB03761>
- 753 Chanton, J. P., Martens, C. S., & Kelley, C. A. (1989). Gas transport from methane-saturated,  
754 tidal freshwater and wetland sediments. *Limnology and Oceanography*, *34*(5), 807–819.  
755 <https://doi.org/10.4319/lo.1989.34.5.0807>
- 756 Chasar, L. S., Chanton, J. P., Glaser, P. H., Siegel, D. I., & Rivers, J. S. (2000). Radiocarbon and  
757 stable carbon isotopic evidence for transport and transformation of dissolved organic carbon,  
758 dissolved inorganic carbon, and CH<sub>4</sub> in a northern Minnesota peatland. *Global Biogeochemical*  
759 *Cycles*, *14*(4), 1095–1108. <https://doi.org/10.1029/1999GB001221>
- 760 Clayer, F., Moritz, A., Gelin, Y., Tessier, A., & Gobeil, C. (2018). Modeling the carbon  
761 isotope signatures of methane and dissolved inorganic carbon to unravel mineralization pathways

- 762 in boreal lake sediments. *Geochimica Et Cosmochimica Acta*, 229, 36–52.  
763 <https://doi.org/10.1016/j.gca.2018.02.012>
- 764 Clayer, F., Gobeil, C., & Tessier, A. (2016). Rates and pathways of sedimentary organic matter  
765 mineralization in two basins of a boreal lake: Emphasis on methanogenesis and methanotrophy:  
766 Methane cycling in boreal lake sediments. *Limnology and Oceanography*, 61(S1), S131–S149.  
767 <https://doi.org/10.1002/lno.10323>
- 768 Cole, J. J., Prairie, Y. T., Caraco, N. F., McDowell, W. H., Tranvik, L. J., Striegl, R. G., et al.  
769 (2007). Plumbing the Global Carbon Cycle: Integrating Inland Waters into the Terrestrial Carbon  
770 Budget. *Ecosystems*, 10(1), 172–185. <https://doi.org/10.1007/s10021-006-9013-8>
- 771 Conrad, R. (1999). Contribution of hydrogen to methane production and control of hydrogen  
772 concentrations in methanogenic soils and sediments. *FEMS Microbiology Ecology*, 28(3), 193–  
773 202. <https://doi.org/10.1111/j.1574-6941.1999.tb00575.x>
- 774 Conrad, R., Claus, P., Chidthaisong, A., Lu, Y., Fernandez Scavino, A., Liu, Y., et al. (2014).  
775 Stable carbon isotope biogeochemistry of propionate and acetate in methanogenic soils and lake  
776 sediments. *Organic Geochemistry*, 73, 1–7. <https://doi.org/10.1016/j.orggeochem.2014.03.010>
- 777 Conrad, R. (2005). Quantification of methanogenic pathways using stable carbon isotopic  
778 signatures: a review and a proposal. *Organic Geochemistry*, 36(5), 739–752.  
779 <https://doi.org/10.1016/j.orggeochem.2004.09.006>
- 780 Conrad, R., Chan, O.-C., Claus, P., & Casper, P. (2007). Characterization of methanogenic  
781 Archaea and stable isotope fractionation during methane production in the profundal sediment of  
782 an oligotrophic lake (Lake Stechlin, Germany). *Limnology and Oceanography*, 52(4), 1393–  
783 1406. <https://doi.org/10.4319/lo.2007.52.4.1393>
- 784 Conrad, R., Claus, P., & Casper, P. (2009). Characterization of stable isotope fractionation during  
785 methane production in the sediment of a eutrophic lake, Lake Dagow, Germany. *Limnology and*  
786 *Oceanography*, 54(2), 457–471. <https://doi.org/10.4319/lo.2009.54.2.0457>
- 787 Conrad, R., Klose, M., Yuan, Q., Lu, Y., & Chidthaisong, A. (2012). Stable carbon isotope  
788 fractionation, carbon flux partitioning and priming effects in anoxic soils during methanogenic  
789 degradation of straw and soil organic matter. *Soil Biology and Biochemistry*, 49, 193–199.  
790 <https://doi.org/10.1016/j.soilbio.2012.02.030>

- 791 Corbett, J. E., Tfaily, M. M., Burdige, D. J., Cooper, W. T., Glaser, P. H., & Chanton, J. P.  
792 (2013). Partitioning pathways of CO<sub>2</sub> production in peatlands with stable carbon isotopes.  
793 *Biogeochemistry*, *114*, 327–340. Retrieved from JSTOR.
- 794 Corbett, J. E., Tfaily, M. M., Burdige, D. J., Glaser, P. H., & Chanton, J. P. (2015). The relative  
795 importance of methanogenesis in the decomposition of organic matter in northern peatlands.  
796 *Journal of Geophysical Research: Biogeosciences*, *120*(2), 280–293.  
797 <https://doi.org/10.1002/2014JG002797>
- 798 Couture, R.-M., Fischer, R., Van Cappellen, P., & Gobeil, C. (2016). Non-steady state diagenesis  
799 of organic and inorganic sulfur in lake sediments. *Geochimica et Cosmochimica Acta*, *194*, 15–  
800 33. <https://doi.org/10.1016/j.gca.2016.08.029>
- 801 Couture, R.-M., Gobeil, C., & Tessier, A. (2008). Chronology of Atmospheric Deposition of  
802 Arsenic Inferred from Reconstructed Sedimentary Records. *Environmental Science &*  
803 *Technology*, *42*(17), 6508–6513. <https://doi.org/10.1021/es800818j>
- 804 Cranwell, P. A. (1981). Diagenesis of free and bound lipids in terrestrial detritus deposited in a  
805 lacustrine sediment. *Organic Geochemistry*, *3*(3), 79–89. [https://doi.org/10.1016/0146-](https://doi.org/10.1016/0146-6380(81)90002-4)  
806 [6380\(81\)90002-4](https://doi.org/10.1016/0146-6380(81)90002-4)
- 807 D'arcy, P. (1993). *Relations entre les propriétés du bassin versant, la morphométrie du lac et la*  
808 *qualité des eaux*. INRS-ETE, Université du Québec, Québec City, Québec, Canada.
- 809 DelSontro, T., Boutet, L., St-Pierre, A., del Giorgio, P. A., & Prairie, Y. T. (2016). Methane  
810 ebullition and diffusion from northern ponds and lakes regulated by the interaction between  
811 temperature and system productivity: Productivity regulates methane lake flux. *Limnology and*  
812 *Oceanography*, *61*(S1), S62–S77. <https://doi.org/10.1002/lno.10335>
- 813 Duan, Z., & Mao, S. (2006). A thermodynamic model for calculating methane solubility, density  
814 and gas phase composition of methane-bearing aqueous fluids from 273 to 523K and from 1 to  
815 2000bar. *Geochimica et Cosmochimica Acta*, *70*(13), 3369–3386.  
816 <https://doi.org/10.1016/j.gca.2006.03.018>
- 817 Egger, M., Rasigraf, O., Sapart, C. J., Jilbert, T., Jetten, M. S. M., Röckmann, T., et al. (2015).  
818 Iron-Mediated Anaerobic Oxidation of Methane in Brackish Coastal Sediments. *Environmental*  
819 *Science & Technology*, *49*(1), 277–283. <https://doi.org/10.1021/es503663z>

- 820 Emrich, K., Ehhalt, D. H., & Vogel, J. C. (1970). Carbon isotope fractionation during the  
821 precipitation of calcium carbonate. *Earth and Planetary Science Letters*, 8(5), 363–371.  
822 [https://doi.org/10.1016/0012-821X\(70\)90109-3](https://doi.org/10.1016/0012-821X(70)90109-3)
- 823 Ettwig, K. F., Butler, M. K., Le Paslier, D., Pelletier, E., Mangenot, S., Kuypers, M. M. M., et al.  
824 (2010). Nitrite-driven anaerobic methane oxidation by oxygenic bacteria. *Nature*, 464(7288),  
825 543–548. <https://doi.org/10.1038/nature08883>
- 826 Feyte, S., Gobeil, C., Tessier, A., & Cossa, D. (2012). Mercury dynamics in lake sediments.  
827 *Geochimica et Cosmochimica Acta*, 82, 92–112. <https://doi.org/10.1016/j.gca.2011.02.007>
- 828 Forster, S., & Graf, G. (1995). Impact of irrigation on oxygen flux into the sediment: intermittent  
829 pumping by *Callinassa subterranea* and “piston-pumping” by *Lanice conchilega*. *Marine*  
830 *Biology*, 123(2), 335–346. <https://doi.org/10.1007/BF00353625>
- 831 Galand, P. E., Yrjälä, K., & Conrad, R. (2010). Stable carbon isotope fractionation during  
832 methanogenesis in three boreal peatland ecosystems. *Biogeosciences*, 7(11), 3893–3900.  
833 <https://doi.org/10.5194/bg-7-3893-2010>
- 834 Gallon, C., Hare, L., & Tessier, A. (2008). Surviving in anoxic surroundings: how burrowing  
835 aquatic insects create an oxic microhabitat. *Journal of the North American Benthological*  
836 *Society*, 27(3), 570–580. <https://doi.org/10.1899/07-132.1>
- 837 Gelwicks, J. T., Risatti, J. B., & Hayes, J. M. (1994). Carbon isotope effects associated with  
838 acetoclastic methanogenesis. *Applied and Environmental Microbiology*, 60(2), 467–472.
- 839 Ghosh, P., & Brand, W. A. (2003). Stable isotope ratio mass spectrometry in global climate  
840 change research. *International Journal of Mass Spectrometry*, 228(1), 1–33.  
841 [https://doi.org/10.1016/S1387-3806\(03\)00289-6](https://doi.org/10.1016/S1387-3806(03)00289-6)
- 842 Gobeil, C., Tessier, A., & Couture, R.-M. (2013). Upper Mississippi Pb as a mid-1800s  
843 chronostratigraphic marker in sediments from seasonally anoxic lakes in Eastern Canada.  
844 *Geochimica et Cosmochimica Acta*, 113, 125–135. <https://doi.org/10.1016/j.gca.2013.02.023>
- 845 Happell, J. D., Chanton, J. P., & Showers, W. J. (1995). Methane transfer across the water-air  
846 interface in stagnant wooded swamps of Florida: Evaluation of mass-transfer coefficients and  
847 isotropic fractionation. *Limnology and Oceanography*, 40(2), 290–298.  
848 <https://doi.org/10.4319/lo.1995.40.2.0290>

- 849 Hare, L. (1995). Sediment Colonization by Littoral and Profundal Insects. *Journal of the North*  
850 *American Benthological Society*, 14, 315. <https://doi.org/10.2307/1467783>
- 851 Hare, L., Carignan, R., & Huerta-Diaz, M. A. (1994). A field study of metal toxicity and  
852 accumulation by benthic invertebrates; implications for the acid-volatile sulfide (AVS) model.  
853 *Limnology and Oceanography*, 39(7), 1653–1668. <https://doi.org/10.4319/lo.1994.39.7.1653>
- 854 Hastie, A., Lauerwald, R., Weyhenmeyer, G., Sobek, S., Verpoorter, C., & Regnier, P. (2018).  
855 CO<sub>2</sub> evasion from boreal lakes: Revised estimate, drivers of spatial variability, and future  
856 projections. *Global Change Biology*, 24(2), 711–728. <https://doi.org/10.1111/gcb.13902>
- 857 Hedges, J. I., & Oades, J. M. (1997). Comparative organic geochemistries of soils and marine  
858 sediments. *Organic Geochemistry*, 27(7), 319–361. <https://doi.org/10.1016/S0146->  
859 [6380\(97\)00056-9](https://doi.org/10.1016/S0146-6380(97)00056-9)
- 860 Hélie, J.-F. (2004). *Géochimie et flux de carbone organique et inorganique dans les milieux*  
861 *aquatiques de l'est du Canada : exemples du Saint-Laurent et du réservoir Robert-Bourassa :*  
862 *approche isotopique* (Phd, Université du Québec à Chicoutimi .). Retrieved from  
863 <https://constellation.uqac.ca/672/>
- 864 Hesslein, R. H. (1976). An in situ sampler for close interval pore water studies1. *Limnology and*  
865 *Oceanography*, 21(6), 912–914. <https://doi.org/10.4319/lo.1976.21.6.0912>
- 866 Holgerson, M. A., & Raymond, P. A. (2016). Large contribution to inland water CO<sub>2</sub> and CH<sub>4</sub>  
867 emissions from very small ponds. *Nature Geoscience*, 9(3), 222–226.  
868 <https://doi.org/10.1038/ngeo2654>
- 869 Holmkvist, L., Ferdelman, T. G., & Jørgensen, B. B. (2011). A cryptic sulfur cycle driven by  
870 iron in the methane zone of marine sediment (Aarhus Bay, Denmark). *Geochimica et*  
871 *Cosmochimica Acta*, 75(12), 3581–3599. <https://doi.org/10.1016/j.gca.2011.03.033>
- 872 Hornibrook, E. R. C., Longstaffe, F. J., & Fyfe, W. S. (1997). Spatial distribution of microbial  
873 methane production pathways in temperate zone wetland soils: Stable carbon and hydrogen  
874 isotope evidence. *Geochimica et Cosmochimica Acta*, 61(4), 745–753.  
875 [https://doi.org/10.1016/S0016-7037\(96\)00368-7](https://doi.org/10.1016/S0016-7037(96)00368-7)
- 876 Hornibrook, E. R. C., Longstaffe, F. J., & Fyfe, W. S. (2000). Evolution of stable carbon isotope  
877 compositions for methane and carbon dioxide in freshwater wetlands and other anaerobic

- 878 environments. *Geochimica et Cosmochimica Acta*, 64(6), 1013–1027.  
879 [https://doi.org/10.1016/S0016-7037\(99\)00321-X](https://doi.org/10.1016/S0016-7037(99)00321-X)
- 880 Jähne, B., Heinz, G., & Dietrich, W. (1987). Measurement of the diffusion coefficients of  
881 sparingly soluble gases in water. *Journal of Geophysical Research: Oceans*, 92(C10), 10767–  
882 10776. <https://doi.org/10.1029/JC092iC10p10767>
- 883 Jørgensen, B. B., & Parkes, R. J. (2010). Role of sulfate reduction and methane production by  
884 organic carbon degradation in eutrophic fjord sediments (Limfjorden, Denmark). *Limnology and*  
885 *Oceanography*, 55(3), 1338–1352. <https://doi.org/10.4319/lo.2010.55.3.1338>
- 886 Joshani, A. (2015). *Investigating organic matter preservation through complexation with iron*  
887 *oxides in Lake Tantaré* (Masters, Concordia University). Retrieved from  
888 <https://spectrum.library.concordia.ca/980434/>
- 889 Kankaala, P., Huotari, J., Tulonen, T., & Ojala, A. (2013). Lake-size dependent physical forcing  
890 drives carbon dioxide and methane effluxes from lakes in a boreal landscape. *Limnology and*  
891 *Oceanography*, 58(6), 1915–1930. <https://doi.org/10.4319/lo.2013.58.6.1915>
- 892 Krzycki, J. A., Kenealy, W. R., DeNiro, M. J., & Zeikus, J. G. (1987). Stable Carbon Isotope  
893 Fractionation by *Methanosarcina barkeri* during Methanogenesis from Acetate, Methanol, or  
894 Carbon Dioxide-Hydrogen. *Applied and Environmental Microbiology*, 53(10), 2597–2599.
- 895 Laforte, L., Tessier, A., Gobeil, C., & Carignan, R. (2005). Thallium diagenesis in lacustrine  
896 sediments. *Geochimica et Cosmochimica Acta*, 69(22), 5295–5306.  
897 <https://doi.org/10.1016/j.gca.2005.06.006>
- 898 Lapham, L., Proctor, L., & Chanton, J. (1999). Using Respiration Rates and Stable Carbon  
899 Isotopes to Monitor the Biodegradation of Orimulsion by Marine Benthic Bacteria.  
900 *Environmental Science & Technology*, 33(12), 2035–2039. <https://doi.org/10.1021/es981158a>
- 901 LaRowe, D. E., & Van Cappellen, P. (2011). Degradation of natural organic matter: A  
902 thermodynamic analysis. *Geochimica et Cosmochimica Acta*, 75(8), 2030–2042.  
903 <https://doi.org/10.1016/j.gca.2011.01.020>
- 904 Lazzaretti, M. A., Hanselmann, K. W., Brandl, H., Span, D., & Bachofen, R. (1992). The role of  
905 sediments in the phosphorus cycle in Lake Lugano. II. Seasonal and spatial variability of

- 906 microbiological processes at the sediment-water interface. *Aquatic Sciences*, 54(3), 285–299.  
907 <https://doi.org/10.1007/BF00878142>
- 908 Lazzaretti-Ulmer, M. A., & Hanselmann, K. W. (1999). Seasonal variation of the microbially  
909 regulated buffering capacity at sediment-water interfaces in a freshwater lake. *Aquatic Sciences*,  
910 61(1), 59–74. <https://doi.org/10.1007/s000270050052>
- 911 Lettmann, K. A., Riedinger, N., Ramlau, R., Knab, N., Böttcher, M. E., Khalili, A., et al. (2012).  
912 Estimation of biogeochemical rates from concentration profiles: A novel inverse method.  
913 *Estuarine, Coastal and Shelf Science*, 100, 26–37. <https://doi.org/10.1016/j.ecss.2011.01.012>
- 914 Matsumoto, G. I. (1989). Biogeochemical study of organic substances in Antarctic lakes.  
915 *Hydrobiologia*, 172(1), 265–299. <https://doi.org/10.1007/BF00031627>
- 916 Meile, C. D., Berg, P., Cappellen, P. S. J., & Tuncay, K. (2005). Solute-specific pore water  
917 irrigation: Implications for chemical cycling in early diagenesis. *Journal of Marine Research*, 63.  
918 <https://doi.org/10.1357/0022240054307885>
- 919 Mook, W. G., Bommerson, J. C., & Staverman, W. H. (1974). Carbon isotope fractionation  
920 between dissolved bicarbonate and gaseous carbon dioxide. *Earth and Planetary Science Letters*,  
921 22(2), 169–176. [https://doi.org/10.1016/0012-821X\(74\)90078-8](https://doi.org/10.1016/0012-821X(74)90078-8)
- 922 Natchimuthu, S., Wallin, M. B., Klemmedtsson, L., & Bastviken, D. (2017). Spatio-temporal  
923 patterns of stream methane and carbon dioxide emissions in a hemiboreal catchment in  
924 Southwest Sweden. *Scientific Reports*, 7(1). <https://doi.org/10.1038/srep39729>
- 925 Niessen, F., Wick, L., Bonani, G., Chondrogianni, C., & Siegenthaler, C. (1992). Aquatic system  
926 response to climatic and human changes: Productivity, bottom water oxygen status, and sapropel  
927 formation in Lake Lugano over the last 10 000 years. *Aquatic Sciences*, 54(3), 257–276.  
928 <https://doi.org/10.1007/BF00878140>
- 929 Norđi, K., Thamdrup, B., & Schubert, C. J. (2013). Anaerobic oxidation of methane in an iron-  
930 rich Danish freshwater lake sediment. *Limnology and Oceanography*, 58(2), 546–554.  
931 <https://doi.org/10.4319/lo.2013.58.2.0546>
- 932 O’Leary, M. H. (1984). Measurement of the isotope fractionation associated with diffusion of  
933 carbon dioxide in aqueous solution. *The Journal of Physical Chemistry*, 88(4), 823–825.  
934 <https://doi.org/10.1021/j150648a041>

- 935 Paraska, D. W., Hipsey, M. R., & Salmon, S. U. (2014). Sediment diagenesis models: Review of  
936 approaches, challenges and opportunities. *Environmental Modelling & Software*, *61*, 297–325.  
937 <https://doi.org/10.1016/j.envsoft.2014.05.011>
- 938 Pick, F. R., Lean, D. R. S., & Nalewajko, C. (1984). Nutrient status of metalimnetic  
939 phytoplankton peaks. *Limnology and Oceanography*, *29*(5), 960–971.  
940 <https://doi.org/10.4319/lo.1984.29.5.0960>
- 941 Pohlman, J. W., Ruppel, C., Hutchinson, D. R., Downer, R., & Coffin, R. B. (2008). Assessing  
942 sulfate reduction and methane cycling in a high salinity pore water system in the northern Gulf of  
943 Mexico. *Marine and Petroleum Geology*, *25*(9), 942–951.  
944 <https://doi.org/10.1016/j.marpetgeo.2008.01.016>
- 945 Pohlman, John W., Riedel, M., Bauer, J. E., Canuel, E. A., Paull, C. K., Lapham, L., et al.  
946 (2013). Anaerobic methane oxidation in low-organic content methane seep sediments.  
947 *Geochimica et Cosmochimica Acta*, *108*, 184–201. <https://doi.org/10.1016/j.gca.2013.01.022>
- 948 Poindexter, C. M., Baldocchi, D. D., Matthes, J. H., Knox, S. H., & Variano, E. A. (2016). The  
949 contribution of an overlooked transport process to a wetland's methane emissions. *Geophysical*  
950 *Research Letters*, *43*(12), 6276–6284. <https://doi.org/10.1002/2016GL068782>
- 951 Raghoebarsing, A. A., Pol, A., van de Pas-Schoonen, K. T., Smolders, A. J. P., Ettwig, K. F.,  
952 Rijpstra, W. I. C., et al. (2006). A microbial consortium couples anaerobic methane oxidation to  
953 denitrification. *Nature*, *440*(7086), 918–921. <https://doi.org/10.1038/nature04617>
- 954 Riisgård, H. U., & Larsen, P. S. (2005). Water pumping and analysis of flow in burrowing  
955 zoobenthos: an overview. *Aquatic Ecology*, *39*(2), 237–258. [https://doi.org/10.1007/s10452-004-](https://doi.org/10.1007/s10452-004-1916-x)  
956 [1916-x](https://doi.org/10.1007/s10452-004-1916-x)
- 957 Sabrekov, A. F., Runkle, B. R. K., Glagolev, M. V., Terentieva, I. E., Stepanenko, V. M.,  
958 Kotsyurbenko, O. R., et al. (2017). Variability in methane emissions from West Siberia's  
959 shallow boreal lakes on a regional scale and its environmental controls. *Biogeosciences*, *14*(15),  
960 3715–3742. <https://doi.org/10.5194/bg-14-3715-2017>
- 961 Sauer, P. E., Miller, G. H., & Overpeck, J. T. (2001). Oxygen isotope ratios of organic matter in  
962 arctic lakes as a paleoclimate proxy: field and laboratory investigations. *Journal of*  
963 *Paleolimnology*, *25*(1), 43–64. <https://doi.org/10.1023/A:1008133523139>

- 964 Saunio, M., Bousquet, P., Poulter, B., Peregon, A., Ciais, P., Canadell, J. G., et al. (2016). The  
965 global methane budget 2000–2012. *Earth System Science Data*, 8(2), 697–751.  
966 <https://doi.org/10.5194/essd-8-697-2016>
- 967 Schindler, D. W., Curtis, P. J., Parker, B. R., & Stainton, M. P. (1996). Consequences of climate  
968 warming and lake acidification for UV-B penetration in North American boreal lakes. *Nature*,  
969 379(6567), 705–708. <https://doi.org/10.1038/379705a0>
- 970 Sivan, O., Schrag, D. P., & Murray, R. W. (2007). Rates of methanogenesis and methanotrophy  
971 in deep-sea sediments. *Geobiology*, 5(2), 141–151. [https://doi.org/10.1111/j.1472-  
972 4669.2007.00098.x](https://doi.org/10.1111/j.1472-4669.2007.00098.x)
- 973 Span, D., Dominik, J., Lazzaretti, M. A., & Vernet, J.-P. (1992). The role of sediments in the  
974 phosphorus cycle in Lake Lugano. I. Geochemical approach. *Aquatic Sciences*, 54(3), 277–284.  
975 <https://doi.org/10.1007/BF00878141>
- 976 Staehr, P. A., Testa, J. M., Kemp, W. M., Cole, J. J., Sand-Jensen, K., & Smith, S. V. (2012).  
977 The metabolism of aquatic ecosystems: history, applications, and future challenges. *Aquatic  
978 Sciences*, 74(1), 15–29. <https://doi.org/10.1007/s00027-011-0199-2>
- 979 Thottathil, S. D., Reis, P. C. J., & Prairie, Y. T. (2019). Methane oxidation kinetics in northern  
980 freshwater lakes. *Biogeochemistry*, 143(1), 105–116. [https://doi.org/10.1007/s10533-019-00552-  
981 x](https://doi.org/10.1007/s10533-019-00552-x)
- 982 Tipping, E. (2002). *Cation binding by humic substances*. Cambridge University Press.
- 983 Turner, A. J., Jacob, D. J., Wecht, K. J., Maasakkers, J. D., Lundgren, E., Andrews, A. E., et al.  
984 (2015). Estimating global and North American methane emissions with high spatial resolution  
985 using GOSAT satellite data. *Atmospheric Chemistry and Physics*, 15(12), 7049–7069.  
986 <https://doi.org/10.5194/acp-15-7049-2015>
- 987 Ullman, W. J., & Aller, R. C. (1982). Diffusion coefficients in nearshore marine sediments 1.  
988 *Limnology and Oceanography*, 27(3), 552–556. <https://doi.org/10.4319/lo.1982.27.3.0552>
- 989 Verpoorter, C., Kutser, T., Seekell, D. A., & Tranvik, L. J. (2014). A global inventory of lakes  
990 based on high-resolution satellite imagery. *Geophysical Research Letters*, 41(18), 6396–6402.  
991 <https://doi.org/10.1002/2014GL060641>

- 992 Wallin, M. B., Campeau, A., Audet, J., Bastviken, D., Bishop, K., Kokic, J., et al. (2018).  
993 Carbon dioxide and methane emissions of Swedish low-order streams—a national estimate and  
994 lessons learnt from more than a decade of observations. *Limnology and Oceanography Letters*,  
995 3(3), 156–167. <https://doi.org/10.1002/lol2.10061>
- 996 Wand, U., Samarkin, V. A., Nitzsche, H.-M., & Hubberten, H.-W. (2006). Biogeochemistry of  
997 methane in the permanently ice-covered Lake Untersee, central Dronning Maud Land, East  
998 Antarctica. *Limnology and Oceanography*, 51(2), 1180–1194.  
999 <https://doi.org/10.4319/lo.2006.51.2.1180>
- 1000 Wang, Y., & Van Cappellen, P. (1996). A multicomponent reactive transport model of early  
1001 diagenesis: Application to redox cycling in coastal marine sediments. *Geochimica et*  
1002 *Cosmochimica Acta*, 60(16), 2993–3014. [https://doi.org/10.1016/0016-7037\(96\)00140-8](https://doi.org/10.1016/0016-7037(96)00140-8)
- 1003 Werth, M., & Kuzyakov, Y. (2010). <sup>13</sup>C fractionation at the root–microorganisms–soil interface:  
1004 A review and outlook for partitioning studies. *Soil Biology and Biochemistry*, 42(9), 1372–1384.  
1005 <https://doi.org/10.1016/j.soilbio.2010.04.009>
- 1006 Whiticar, M. J., Faber, E., & Schoell, M. (1986). Biogenic methane formation in marine and  
1007 freshwater environments: CO<sub>2</sub> reduction vs. acetate fermentation—Isotope evidence.  
1008 *Geochimica et Cosmochimica Acta*, 50(5), 693–709. [https://doi.org/10.1016/0016-](https://doi.org/10.1016/0016-7037(86)90346-7)  
1009 [7037\(86\)90346-7](https://doi.org/10.1016/0016-7037(86)90346-7)
- 1010 Whiticar, M. J. (1999). Carbon and hydrogen isotope systematics of bacterial formation and  
1011 oxidation of methane. *Chemical Geology*, 161(1), 291–314. [https://doi.org/10.1016/S0009-](https://doi.org/10.1016/S0009-2541(99)00092-3)  
1012 [2541\(99\)00092-3](https://doi.org/10.1016/S0009-2541(99)00092-3)
- 1013 Whiticar, M. J., & Faber, E. (1986). Methane oxidation in sediment and water column  
1014 environments—Isotope evidence. *Organic Geochemistry*, 10(4), 759–768.  
1015 [https://doi.org/10.1016/S0146-6380\(86\)80013-4](https://doi.org/10.1016/S0146-6380(86)80013-4)
- 1016 Wuebbles, D. J., & Hayhoe, K. (2002). Atmospheric methane and global change. *Earth-Science*  
1017 *Reviews*, 57(3), 177–210. [https://doi.org/10.1016/S0012-8252\(01\)00062-9](https://doi.org/10.1016/S0012-8252(01)00062-9)Deng, A., & Stauffer,  
1018 D. R. (2006), On improving 4-km mesoscale model simulations. *Journal of Applied Meteorology*  
1019 *and Climatology*, 45(3), 361–381. doi:10.1175/JAM2341.1